THE ASTRONOMICAL JOURNAL, 118:208–235, 1999 July

WFPC2 OBSERVATIONS OF COMPACT STAR CLUSTER NUCLEI IN LOW-LUMINOSITY SPIRAL GALAXIES[1]

LYNN D. MATTHEWS,[2,3] JOHN S. GALLAGHER III,[4] JOHN E. KRIST,[5] ALAN M. WATSON,[6] CHRISTOPHER J. BURROWS,[5] RICHARD E. GRIFFITHS,[7] J. JEFF HESTER,[8] JOHN T. TRAUGER,[9] GILDA E. BALLESTER,[10] JOHN T. CLARKE,[10] DAVID CRISP,[9] ROBIN W. EVANS,[9] JOHN G. HOESSEL,[4] JON A. HOLTZMAN,[11] JEREMY R. MOULD,[12] PAUL A. SCOWEN,[8] KARL R. STAPELFELDT,[9] AND JAMES A. WESTPHAL[13]

Received 1998 September 4; accepted 1999 March 22

ABSTRACT

We have used the Wide Field Planetary Camera 2 (WFPC2) aboard the *Hubble Space Telescope* to obtain F450W and F814W (*B*- and *I*-band) observations of the compact star cluster nuclei of the nearby, late-type, low-luminosity spiral galaxies NGC 4395, NGC 4242, and ESO 359-029. In addition, we analyze archival WFPC2 observations of the compact star cluster nucleus of M33. All of these galaxies are structurally diffuse, with moderately low surface brightnesses and little or no discernible bulge component. Here we present a comparative analysis of the structural and photometric properties of their nuclei. NGC 4395 contains a Seyfert 1 nucleus; M33 has some signatures of weak nuclear activity; the other two galaxies are not known to be active. All of the nuclei have $M_I \sim -11$; hence these represent a little explored low-luminosity extension of the galactic nuclear activity sequence in a class of host galaxy not traditionally associated with galactic nuclear phenomena. These kinds of compact nuclei appear to be quite common in low luminosity, late-type spirals. Our Planetary Camera 2 images partially resolve the nuclei of all four galaxies. A simple model consisting of an isothermal sphere plus a point source provides a good model for the observed radial intensity distribution in all cases and permits an exploration of the underlying nuclear structures and spatial scales. Despite their low luminosities, all of the nuclei are very compact. In all cases the luminosity densities are increasing at small radii to the resolution limit of our data. In spite of having similar size scales and luminosities, the nuclei in our sample span a wide range of $B-I$ color. This may be a signature of different evolutionary phases. The M33 nucleus exhibits complex structure; its isophotes are elongated, and it has a possible jetlike component. The Seyfert nucleus of NGC 4395 has an extremely blue color ($B-I = -0.16$) and is the most structurally complex nucleus in our sample. Circularly symmetric fits to its underlying structure reveal a distinct bipolar pattern. A pair of bright filaments located on one side of the nucleus are probably due to [O III] emission from gas within a nuclear ionization cone. NGC 4395 appears to contain an underlying normal star cluster nucleus that is hosting activity. NGC 4242 shows evidence of a slightly elongated, bar-shaped feature at its center. The ESO 359-029 nucleus appears relatively symmetric and featureless at the resolution limit of our data, but it is clearly very compact. The circumnuclear environments of all four of our program galaxies are extremely diffuse, have only low to moderate star formation, and appear to be devoid of large quantities of dust. The central gravitational potentials of the galaxies are also quite shallow, making the origin of these types of "naked" nuclei problematic.

Key words: galaxies: active — galaxies: nuclei — galaxies: spiral

1. INTRODUCTION

1.1. *Background*

Compact galactic nuclei are a common but still poorly understood feature of many, if not most, spiral galaxies, including our own Milky Way. Such nuclei are regions only a few parsecs or less in diameter but that have complex structures and sometimes produce energy outputs equal to a significant fraction of the total galaxy luminosity. For the present work we define a *compact nucleus* as a nonstellar, pointlike light enhancement at or near the center of a galaxy whose brightness is in excess of an extrapolation of the galaxy light profile from the surrounding regions (e.g., Phillips et al. 1996) and which is dynamically distinct from the surrounding galaxy disk. Compact nuclei are not simply nuclear H II regions, although in some cases, they may be one component of a composite nucleus—i.e., they may be

[1] Based on observations with the NASA/ESA *Hubble Space Telescope*, obtained at the Space Telescope Science Institute, which is operated by the Association of Universities for Research in Astronomy, Inc., under NASA contract NAS 5-26555.

[2] Department of Physics and Astronomy, State University of New York at Stony Brook, Stony Brook, NY 11794-3800.
[3] Current address: National Radio Astronomy Observatory, 520 Edgemont Road, Charlottesville, VA 22903; lmatthew@nrao.edu.
[4] Department of Astronomy, University of Wisconsin, 475 North Charter Street, Madison, WI 53706-1582.
[5] Space Telescope Science Institute, 3700 San Martin Drive, Baltimore, MD 21218.
[6] Instituto de Astronomía, Universidad Nacional Autónoma de México, J. J. Tablada 1006, 58090 Morelia, Michoacán, Mexico.
[7] Department of Physics, Carnegie Mellon University, 5000 Forbes Avenue, Wean Hall, Pittsburgh, PA 15213.
[8] Department of Physics and Astronomy, Arizona State University, Tyler Mall, Tempe, AZ 85287.
[9] Jet Propulsion Laboratory, MS 183-900, California Institute of Technology, Pasadena, CA 91109.
[10] Department of Atmospheric, Oceanic, and Space Sciences, University of Michigan, 2455 Hayward, Ann Arbor, MI 48109.
[11] Department of Astronomy, New Mexico State University, Box 30001, Department 4500, Las Cruces, NM 88003-8001.
[12] Mount Stromlo and Siding Spring Observatories, Australian National University, Weston Creek Post Office, ACT 2611, Australia.
[13] Division of Geological and Planetary Sciences, California Institute of Technology, Pasadena, CA 91125.

embedded in a nuclear H II region, a nuclear starburst region, or a nuclear disk (e.g., Filippenko 1989; van den Bergh 1995; Ford et al. 1998). Compact galactic nuclei include both "active galactic nuclei" or "AGNs" (i.e., QSOs, Seyferts, and LINERs), which exhibit characteristic emission lines and nonstellar spectral energy distributions, as well as "compact star cluster nuclei," whose properties can be accounted for by dense concentrations of stars. Compact star cluster nuclei are the densest known stellar systems, with even modest examples containing a mass of more than $10^6\ M_\odot$ within a few parsecs radius (e.g., Lauer et al. 1998, hereafter L98). Star cluster nuclei differ from scaled-up versions of normal dense star clusters in that they exhibit a wider range of stellar ages, quantities of associated dense gas, and sometimes evidence for the existence of central massive black holes. Possible evolutionary links between AGNs and compact star cluster nuclei are still widely debated (e.g., Norman & Scoville 1988; Filippenko 1992; Williams & Perry 1994; and references therein).

Compact galactic nuclei can be difficult to pick out even in nearby galaxies. Studies from the ground are limited by the effects of seeing and confusion with bright bulges or regions of enhanced star formation in galaxy centers. Moreover, in the past, owing to the limited dynamic range of photographic plates, exposures that revealed the outer structures of galaxies often overexposed the nuclear regions, thus obscuring compact nuclear sources (e.g., van den Bergh 1995). For some time it was accepted that compact nuclei were mainly limited to dwarf spheroidal galaxies (e.g., Binggeli, Sandage, & Taraenghi 1984; Binggeli & Cameron 1991) and to elliptical galaxies or early-type spiral bulges in which massive (10^6–$10^7\ M_\odot$) black holes appear to be commonplace (e.g., Ford et al. 1998; van der Marel 1998; and references therein). However, high-quality photographic plates and high dynamic range CCD images, where the nuclear regions of galaxies are not "burned in," have helped to change our perceptions on the range in properties of compact nuclei and on the types of galaxies that may harbor them (e.g., van den Bergh 1995).

In particular, it has become evident that true compact nuclei are common in low-luminosity, late-type (Scd–Sdm) spiral disks that lack a bulge component (i.e., "extreme late-type spirals"). Although the compact nuclei of extreme late-type spirals are often relatively faint ($M_V \geq \sim -12$), in nearby galaxies they become readily detectable even from the ground under normal ($\sim 1''$) seeing conditions, since confusion from bulges or brilliant circumnuclear disks is minimal, and dust obscuration is often low.

For example, Matthews & Gallagher (1997) noted the existence of moderate- to low-luminosity compact, semi-stellar nuclei in 10 of 49 nearby, extreme late-type spirals they imaged from the ground. In a Snapshot survey with the *Hubble Space Telescope* (*HST*), Phillips et al. (1996) also found compact nuclei in a number of nearby, late-type, low-luminosity spirals (see also Carollo et al. 1997). Compact nuclei may be common in pure disk galaxies at least to moderate redshifts. Sarajedini et al. (1996) found that in a magnitude-limited survey ($I \leq 21.5$), 84 of 825 galaxies contained unresolved nuclear sources. Of these, 57% of the host galaxies could be adequately modeled by an exponential disk alone, with no bulge component (see also Sarajedini 1996).

The bulk of the compact nuclei in nearby extreme late-type spirals appear to be of the "compact star cluster" variety (e.g., Shields & Filippenko 1992; Phillips et al. 1996). Nearby examples include the nucleus of the Local Group Scd spiral M33 (e.g., Kormendy & McClure 1993, hereafter KM; L98) and the nucleus of the Sd spiral NGC 7793 (Díaz et al. 1982; Shields & Filippenko 1992). However, in a ground-based spectroscopic survey of 43 Scd and later nucleated galaxies, Ho (1996) reported that a surprising 16% of these objects showed evidence for nuclear activity (i.e., Seyfert, LINER, or "transition" nuclei).

Among the handful of examples of compact nuclei in low-luminosity disk galaxies that have been studied in detail, there have been other surprises. One of the nearest QSOs (0351+026 at $z = 0.036$) was found by Bothun et al. (1982a, 1982b) to lie within a faint ($M_V = -18.6$),[14] blue, moderately low surface brightness disk galaxy. Moreover, it is interacting with a nucleated, low surface brightness, gas-rich galaxy with $M_V \sim -17.5$ (Bothun et al. 1982a). Kunth, Sargent, & Bothun (1987) were the first to image the galaxy G1200−2038 associated with a Seyfert 2 nucleus. The host galaxy is a very small, faint dwarf galaxy ($D_{25} \approx 6$ kpc and $M_V = -16.8$). The detailed morphology of this galaxy is uncertain, but it is well represented by a pure exponential disk, and its small physical size and low luminosity are consistent with an extreme late-type spiral galaxy (cf. Matthews & Gallagher 1997). In spite of the properties of the host galaxy, the nucleus of G1200−2038 has a luminosity $M_V \sim -16.1$, yielding a ratio of nuclear to host galaxy luminosity typical of much more luminous AGNs. Such cases as these may hold important clues as to how different "flavors" of active nuclei are related, and they raise the question of whether compact nuclei in nearby extreme late-type spirals have special characteristics or perhaps were much more powerful objects in the past that have since run out of fuel. Furthermore, since moderate- to low-luminosity Sd–Sm spirals are the most common class of disk galaxy (van der Kruit 1987), if nuclear activity was commonplace in these objects, it may make a significant contribution to the soft X-ray background (e.g., Koratkar et al. 1995).

However, the majority of nuclei in nearby extreme late-type spirals appear to be either weakly active or nonactive, and these galaxies therefore furnish examples of the little explored low-luminosity regime for galactic nuclei and nuclear activity. The investigation of this faint end of the galactic nuclear activity sequence is critical for constraining the origin and evolution of compact nuclei and nuclear activity, as well as the physical processes that power them, since the existence of compact nuclei in small diffuse galaxies with weak central potentials and no bulge component is difficult to explain in light of current models for the origin of compact galactic nuclei and nuclear activity (see § 6). Nonetheless, exploration of these systems is largely just beginning (e.g., Filippenko & Sargent 1985; Ho, Filippenko, & Sargent 1995a, 1997a, 1997b; Koratkar et al. 1995; Maiolino & Rieke 1995; Sarajedini et al. 1996). Still unanswered questions include: Do all star cluster nuclei contain central black holes? Are young stellar populations centrally located within nuclei? How do structures and spatial scales compare between active and nonactive nuclei? What is the minimum luminosity for an active nucleus? Because confusion with dust, light from the bulge, and bright circumnuclear material are minimized, detailed studies of the nuclei

[14] $H_0 = 75\ \mathrm{km\ s^{-1}\ Mpc^{-1}}$ is assumed throughout this work.

of nearby extreme late-type spirals can help to afford unique insights to many of these problems.

By studying the nuclei of extreme late-type spirals, we can also hope to further our understanding of the role of the host galaxy in provoking and sustaining nuclear activity and explore what relationships may exist between morphology, luminosity, or other global properties of the host galaxy and its nuclear characteristics. For example, Filippenko & Sargent (1989) discovered the faintest Seyfert 1 nucleus yet known ($M_B \sim -11$) in NGC 4395, one of the objects we explore further in the present study. We also investigate the "normal" nuclei in the Sd/Sdm galaxies NGC 4242 and ESO 359-029 and analyze the nearby M33 nucleus as a comparison object.

1.2. *Past Observational Limitations and Progress from HST*

Constraining the physics of compact galactic nuclei requires resolution of their structures and measurements of their physical sizes. However, since half-light radii are typically ≤ 10 pc, even the closest spiral galaxy nuclei are difficult to resolve from the ground with conventional observing techniques (e.g., Gallagher, Goad, & Mould 1982; Nieto et al. 1986; Mould et al. 1989; KM). In general, space-based observations with image quality of $\leq 0\farcs1$ are needed to procure sufficiently detailed information to advance our understanding of these objects. The first such observations were supplied for M31 by the Stratoscope II balloon-borne telescope (Light, Danielson, & Schwarzschild 1974). More extensive data on structures of external spiral galaxy nuclei have come from ultraviolet (UV) and optical images obtained with the cameras aboard the *HST* that now achieve $\sim 0\farcs05$ angular resolution.

Even before its spherical aberration was corrected, the *HST* displayed its resolving power by revealing that M31 has a double nucleus (Lauer et al. 1993), showing that compact nuclei are common in the UV (e.g., Fabbiano, Fassnacht, & Trinchieri 1994; Maoz et al. 1995), and by providing initial measures of galactic nuclear structures (e.g., Crane et al. 1993; Lauer et al. 1993, 1995; King, Stanford, & Crane 1995; Ford et al. 1992; Phillips et al. 1996). These results have been confirmed with optical and mid-UV images from the corrected optics of the Wide Field Planetary Camera 2 (WFPC2) and the COSTAR-corrected Faint Object Camera (e.g., Colina et al. 1997; Devereux, Ford, & Jacoby 1997). Aberration-corrected *HST* images of the centers of a few nearby spirals show that typical galaxy nuclei are often unresolved in the UV, especially in galaxies with some evidence for activity. In the visible, nuclei of spirals can have complex surroundings (e.g., as in M100) and range in size from less than 1 pc (e.g., M81, as measured by Devereux et al. 1997) to core radii of 1.4 and 3.7 pc, respectively, for the P1 and P2 double nuclei of M31 (Lauer et al. 1993; L98).

1.3. *New Goals*

In this paper we present a WFPC2 investigation of the galactic nuclei of three extreme late-type, Sd–Sdm spiral galaxies. We also present an analysis of WFPC2 data of the nucleus of our closest Scd spiral neighbor, M33, in order to form a comparative framework for our analysis. All of these galaxies are dominated by their stellar disks and have little or no bulge component. Our objectives are to study the optical structures, colors, and spatial scales of the low-luminosity, "naked" galactic nuclei found in these galaxies and to compare these results with other compact galactic nuclei. A preliminary version of this work was presented by Matthews et al. (1996).

The global properties of our program galaxies are described in Table 1. Our first target, NGC 4395, is an SAd III–IV Seyfert 1 galaxy (Filippenko & Sargent 1989; Filippenko, Ho, & Sargent 1993). NGC 4242 (SABd III) is morphologically similar to NGC 4395 (cf. Sandage & Bedke 1994), although slightly more distant, and its optically prominent nucleus does not appear to be active (Ho et al. 1995a). The less luminous, nucleated extreme late-type galaxy, ESO 359-029 (Sdm) was selected from the sample of Matthews & Gallagher (1997; see also Sandage & Fomalont 1993) and is one of the lowest luminosity disk galaxies ($M_B = -15.1$) known to have a nucleus. ESO 359-029 does not appear to be active, but a long-slit spectrum (Matthews 1998) reveals the kinematic signature of a compact central mass concentration at the location of the nucleus. Last, M33 (SAcd III) and its nucleus have similar luminosities to our other targets, but because it is nearby, it is well resolved and has been previously extensively investigated at multiple wavelengths (see L98). It therefore serves as an excellent comparison object, a check on the validity of our analysis techniques, as well as a guide for the interpretation of our results.

2. OBSERVATIONS

Images of NGC 4395, NGC 4242, and ESO 359-029 were obtained for this program by the WFPC2 Investigation Definition Team. The observations are summarized in

TABLE 1

PROPERTIES OF THE TARGET GALAXIES

Galaxy (1)	Type (2)	M_B (3)	$B-V$ (4)	Distance (5)	i (deg) (6)	$M_{\rm H\,I}$ ($M_\odot$) (7)	W_{20} (km s^{-1}) (8)	A_B (9)	References (10)
NGC 4395	SAd III–IV	−17.1	0.46	2.6	38	1.6×10^9	131	0.01	1, 2, 3
NGC 4242	SABd III	−17.9	0.54	7.5	50	6.4×10^8	142	0.0	1
ESO 359-029.....	SAd/SAdm	−15.1	0.62	10.1	56	6.8×10^7	141	0.0	4, 5, 6
M33.....	SAcd III	−18.2	0.55	840	56	1.3×10^9	204	0.28	1, 7, 8

NOTES.—Col. (1): Galaxy name. Col. (2): Hubble type. Col. (3): Absolute B magnitude, corrected for Galactic extinction and assuming distances in col. (5). Col. (4): $B-V$ color. Col. (5): Distance in megaparsecs, except for M33, which is in kiloparsecs. Col. (6): Inclination. Col. (7): Neutral hydrogen mass. Col. (8): H I profile velocity width, measured at 20% peak maximum. Col. (9): B-band Galactic extinction in magnitudes. Col. (10): References.

REFERENCES.—(1) Tully 1988; (2) Rowan-Robinson 1985; (3) Sandage & Bedke 1994; (4) Matthews & Gallagher 1997; (5) Matthews et al. 1998; (6) Lauberts & Valentijn 1989; (7) van den Bergh 1991; (8) Freedman, Wilson, & Madore 1991.

TABLE 2

SUMMARY OF PLANETARY CAMERA 2 OBSERVATIONS

Galaxy (1)	Observation (2)	PI (3)	Date of Observation (4)	λ Observation (5)	Exposure Times (s) (6)	Pixel Scale (pc) (7)
NGC 4395	u2rf0101-0106	Trauger	1995 Dec 5	F450W, F814W	860, 660	0.57
NGC 4242	u2rf0201-0206	Trauger	1995 Dec 5	F450W, F814W	960, 660	1.65
ESO 359-029.....	u2rf0401-0406	Trauger	1995 Jul 22	F450W, F814W	860, 660	2.23
M33[a].....	u2lg0501-050c	Westphal	1995 Jan 19	F555W, F814W	20, 10	0.18

NOTES.—All images were obtained using the Planetary Camera 2 CCD of the WFPC2 aboard the *HST*. Col. (1): Galaxy name. Col. (2): Space Telescope Science Institute image reference numbers used for the observations analyzed in the present work. Col. (3): Principle investigator for the observations. Col. (4): Date of observations. Col. (5): Filters used for observations. Col. (6): Exposure times in each of the respective filters listed in col. (5). Col. (7): Approximate linear size in parsecs subtended by one 0.″0455 PC2 pixel at the distance of the galaxy.

[a] M33 images were obtained from the *HST* archives maintained by the Canadian Astronomical Data Centre.

Table 2. The nuclei of the galaxies were observed with the Planetary Camera 2 (PC2), which gives a scale of 0.″0455 per pixel on an 800 × 800 pixel Loral CCD. We used a gain of 7 e^- per data number (DN), and the CCD was operated at a temperature of −88°C. More details regarding WFPC2 can be found in, e.g., Trauger et al. (1994), Holtzman et al. (1995a), or Biretta et al. (1996).

Since our program was limited to one orbit per galaxy, we obtained one short and two moderate, CR-SPLIT exposures for each object in the F450W (WFPC2 broad *B*-band) and F814W (WFPC2 broad *I*-band) filters. The short exposures were made to avoid saturated pixels in the bright centers of the nuclei. Total exposure times for each object are given in Table 2. The F450W filter includes the Hβ and

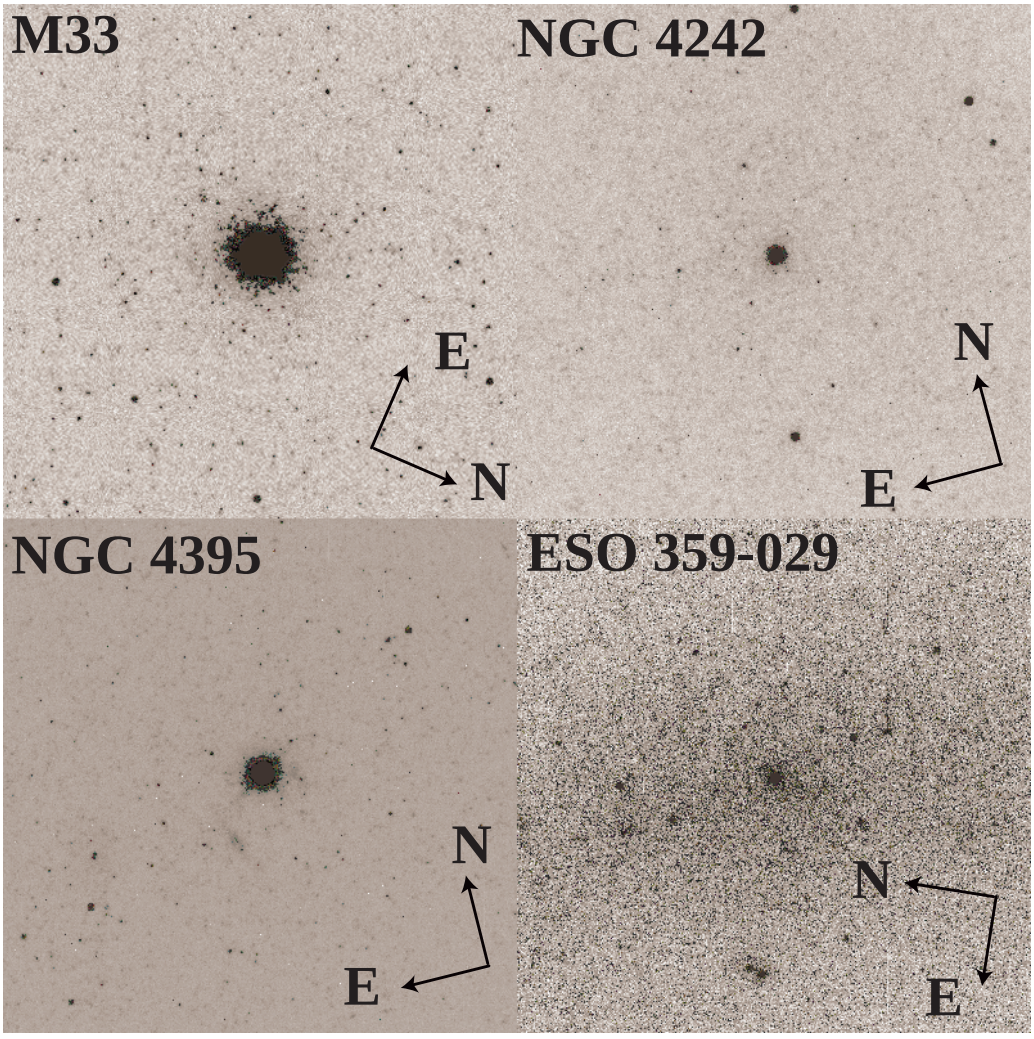

FIG. 1.—F814W-band WFPC2 images of our four program nuclei. Field sizes are roughly 11.″6 × 11.″6. Image orientations are given by the arrows. All gray scales are linear.

[O III] $\lambda\lambda$4959, 5007 emission lines, which can be very strong near an AGN. Together, F450W and F814W give us a good color baseline. The data were reduced following the precepts of Holtzman et al. (1995a) and using the approach discussed by Watson et al. (1996) for removing cosmic rays. Calibrations of magnitudes and fluxes are based on the system described by Holtzman et al. (1995b).

The data for M33 were obtained from the archives of the Canadian Astronomical Data Centre. These data consist of recalibrated WFPC2 images taken in the F555W (WFPC2 V-band) and F814W filters and were pipeline calibrated and combined in IRAF[15] to eliminate cosmic rays. The archival observations that we used are also summarized in Table 2. The F814W images of each of our target nuclei are shown in Figure 1.

3. A METHOD FOR CHARACTERIZING THE BRIGHTNESS PROFILES OF THE NUCLEI

3.1. *Model Fits*

In order to obtain information about the underlying structure and spatial scales of the nuclei of our target galaxies, we have produced simple models of their light distributions by fitting the data with combinations of point sources plus extended components with simple analytical forms. Our approach is motivated by the need to extract information from objects that are only slightly resolved and to contend with the undersampling of the PC2. Both of these effects limit the ability to reconstruct uniquely brightness distributions of small angular size sources, such as nuclei (e.g., Wildey 1992; Bouyoucef, Fraix-Burnet, & Roques 1997). For nonactive or weakly active nuclei, our models are motivated physically by the structure of the Milky Way nucleus (e.g., Mezger, Duschl, & Zylka 1996) as it would appear at larger distances. Our models are also appropriate for star cluster nuclei hosting AGNs (e.g., Norman & Scoville 1988; Perry & Williams 1993).

Our modeling approach has the advantage of requiring a minimum number of free parameters while at the same time yielding measures of the characteristic sizes of the nuclei and limits on their central luminosity densities. Because our approach does not rely on deconvolution methods, we avoid the addition of noise and spurious structures at small radii that can be introduced by such techniques (e.g., Michard 1996). Deconvolution is especially problematic for undersampled PC2 data, where the solution is strongly dependent upon the pixel phase of the adopted point-spread function (PSF) (see Hasan & Burrows 1995). Moreover, if the structures of nuclei are discontinuous at small radii and discrete pointlike features are present near their centers, such information would not necessarily be recovered through deconvolution techniques (see Sams 1995). Finally, our modeling approach allows us to locate off-center or unsymmetrical features in our nuclei.

The point-source contribution for our fits was modeled using the Tiny Tim Version 4.1 software (Krist 1996) to produce a PSF for the PC2 for the appropriate filter, approximate $B-V$ color, and the spatial position on the PC2 CCD. The PSF was subsampled by a factor of 3 and then interpolated in order provide finer shifting and thus improve our ability to align the model PSF with the observations. In all cases jitter corrections were negligible.

For the extended component of our fits, we considered several different analytical forms for the brightness distribution (see Table 3). Note that for $\gamma = 2.0$, model 4 becomes the standard Hubble-Reynolds law (Reynolds 1913; Hubble 1930). For $\gamma = 0.25$, model 6 reduces to the de Vaucouleurs $R^{1/4}$ law (de Vaucouleurs 1948), and in the case of $\gamma = 2.0$, model 8 is an isothermal sphere (also known as a "modified Hubble" or "analytical King model"; see Binney & Tremaine 1987). Model 7 (King 1962, 1966) also reduces to an isothermal sphere in the limit $c \equiv \log (r_t/r_c) \rightarrow \infty$. As we discuss below, more complex models with additional free parameters cannot be adequately constrained by the present data.

For each of our target galaxies we attempted fits to the nuclei using models of three categories: (1) pure PSFs; (2) pure extended models of each of the types listed in Table 3; (3) combinations of a PSF and extended models. For cases 2 and 3, it was necessary to convolve the extended component model with our Tiny Tim model of the intrinsic PSF of the optics and to account for the effects of pixel scattering on its observed appearance. We accomplished this transformation

[15] IRAF is distributed by the National Optical Astronomy Observatories, operated by the Associated Universities for Research in Astronomy, Inc., under cooperative agreement with the National Science Foundation.

TABLE 3

ANALYTIC FITTING FUNCTIONS USED FOR "EXTENDED MODELS"

Equation (1)	Function (2)	Form (3)	Free Parameters (4)	Fitted Parameters (5)
(1)	Exponential disk	$I(r) = I_0 \exp [-(r/r_h)]$	2	I_0, r_h
(2)	Power law	$I(r) = I_0(r/r_p)^{-\gamma}$	3	I_0, r_p, γ
(3)	Hubble-Reynolds	$I(r) = I_0[1 + (r/r_0)]^{-2}$	2	I_0, r_0
(4)	Generalized Hubble-Reynolds	$I(r) = I_0[1 + (r/r'_0)]^{-\gamma}$	3	I_0, r'_0, γ
(5)	de Vaucouleurs $R^{1/4}$	$I(r) = I_0 \exp (- 7.67[(r/r_e)^{0.25} - 1])$	2	I_0, r_e
(6)	Generalized de Vaucouleurs	$I(r) = I_0 \exp (- 7.67[(r/r'_e)^{\gamma} - 1])$	3	I_0, r'_e, γ
(7)	King	$I(r) = I_0[(1/[1 + (r/r_c)^2]^{0.5}) - (1/[1 + (r_t/r_c)^2]^{0.5})]^{-2}$	3	I_0, r_c, r_t
(8)	Modified King	$I(r) = I_0[1 + (r/r'_c)^{\gamma}]^{-1}$	3	I_0, r_c, γ
(9)	Isothermal sphere	$I(r) = I_0[1 + (r/r_c)^2]^{-1}$	2	I_0, r_c

NOTES.—The number of free parameters listed in col. (4) and the list of fitted parameters in col. (5) refer to quantities to be determined for the particular model in addition to the background level and the model centroid. Definition of symbols: (1) r_h: exponential scale length; (2) r_p: a characteristic scale; (3) r_0: "structural length," i.e., the radius at which surface brightness falls to one-quarter of its central value; (4) r'_0: a characteristic scale length; (5) r_e: "effective radius" that contains one-half of the total integrated light; (6) r'_e: a scaling radius; (7) r_c: "core radius" at which intensity falls to one-half its peak value; r_t: tidal radius at which intensity drops to zero; (8) r'_c: a characteristic radius; (9) r_c: "core radius" at which intensity falls to one-half its peak value. In all cases, $I(r)$ denotes intensity as a function of radius, I_0 is a normalization factor, and γ denotes some unknown power.

by subsampling the generated extended model component, convolving it with the central 9×9 pixels of the subsampled Tiny Tim PSF, rebinning to normal sampling, and finally, convolving the extended model with the pixel scattering kernel.

3.2. *Fitting Procedure*

Our fitting procedure began with inputting initial guesses for the various free parameters in the models. Any or all of the free parameters listed in Table 3 were allowed to vary during fitting. In addition, we could also allow the peak intensity of the PSF ($I_{\rm PSF}$) and the fractional pixel shift of both the PSF center, $(x_c, y_c)_{\rm PSF}$, and of the extended component center, $(x_c, y_c)_{\rm ext}$, to vary.

With our software, fitting was accomplished using a two-dimensional nonlinear least-squares technique based on the CURFIT program of Bevington (1969). This method employs the Marquardt (1963) algorithm, which combines a gradient search and an analytical solution derived from linearizing the fitting function. Individual pixels were weighted using Poisson statistics. In all cases, a χ^2 goodness-of-fit criterion was used to evaluate the quality of the models. For each fit, we show a two-dimensional representation of goodness-of-fit as Merit = (Data − Fit)^2 × Weight. These are a useful tool for comparing the goodness of fit between different nuclei, since owing to normalization uncertainties, the absolute values of the derived χ^2 measures are difficult to compare directly. Outputs from our fits included values for the free parameters for each model from Table 3, as well as for $I_{\rm PSF}$, $(x_c, y_c)_{\rm ext}$, $(x_c, y_c)_{\rm PSF}$, the background level, and the integrated fluxes of the PSF and the extended component contributions to the final fit.

To estimate the sensitivity of our fits to effects of time variability in the PSF and camera focus, to mismatches between the true PSF and our model PSF, and to the relative strengths of the underlying PSF and extended components, we generated test images composed of an *observed* F814W PSF with different focus values added to a model extended component. For the extended model, we adopted a generalized Hubble-Reynolds law (model 4) with $r'_0 = 1.0$ or 1.5 pixels and $\gamma = 2.0$ or 2.5. We tested focus offsets of up to 5 μm (i.e., $1/20\lambda$), which is the maximum amount of defocus we expect to see in real images (Biretta et al. 1996). We then attempted to fit these test images with our fitting software using a nominal Tiny Tim PSF in perfect focus, plus a generalized Hubble-Reynolds extended component. We repeated this procedure on test images where the relative strength of the PSF component $I_{\rm PSF}$ to the extended component I_0 ranged from 10 to 0.35. Regardless of focus, we found the fits output by our modeling software to underestimate the value of $I_{\rm PSF}$ by ~3%–5%. I_0 was accurately determined when $I_{\rm PSF}/I_0 = 0.35$ but was overestimated by up to 33% in the case of $I_{\rm PSF}/I_0 = 10$. Errors on γ range from 0 to 10%, depending upon both the ratio $I_{\rm PSF}/I_0$ and the true γ of the test image. Finally, for the in-focus test images, r'_0 was systematically underestimated by 2%–6%, while in the defocused test images, r'_0 was overestimated by 2%–26%, depending on $I_{\rm PSF}/I_0$ and the true underlying r'_0 of the test image. In the discussions that follow, we use the above results as partial guidelines for estimating the uncertainty of the fit parameters derived from our modeling technique.

As a second test of the accuracy of the PSF models produced from Tiny Tim, we attempted to use appropriately scaled versions of the Tiny Tim models to subtract field stars from our observed image frames. We found the Tiny Tim models to accurately subtract the stars to within ~2 σ. These residuals are consistent with those expected from the effects of Poisson noise and the large-angle scattering in the WFPC2 camera that is not modeled by Tiny Tim. We adopt the Tiny Tim model PSFs for our nuclear fits rather than using an observed PSF from each frame, since the observed point sources on our frames are of rather low signal-to-noise. In addition, because the PC2 PSF is position-dependent, the adopted PSF must be interpolated to match the location of the observed nucleus. This can be done with much greater accurately with a subsampled Tiny Tim PSF than with an observed PSF.

From our tests we deduced the optimal extraction box size for fitting to be 31×31 pixels. This size included the bulk of the signal from each nucleus, while excluding most of the light from the large-angle scattering halo. Because M33 is brighter and better resolved (and hence less sensitive to uncertainty in the PSF halo), we extended its box size to 61×61 pixels. Modest changes in box size caused maximum changes of a few percent in our derived fit parameters.

3.2.1. *Pure PSF Fits*

To assess how well we had resolved our nuclei, we attempted fits to the nuclei of all program images using a pure point source (i.e., a Tiny Tim PSF). We find that *none* of the nuclei of our target galaxies can be adequately fit by a pure PSF. Figure 2 illustrates this for the most distant nucleus in our sample, ESO 359-029. Clearly a PSF properly scaled to fit the profile wings grossly overestimates the central intensity. The mismatch is even more extreme in the other three cases. This implies that *we have partially resolved the nuclei of all four of our program galaxies.* For NGC 4395 and M33, the resolution is evident even from visual inspection of the images.

3.2.2. *Pure Extended Component Fits*

As a second step, we attempted to fit all four of our program nuclei using simple analytical brightness distribution models of the forms given in Table 3. We found that several of these models (1, 3, 4, 6, 7, 8, and 9) could adequately fit the outer wings of the nuclear brightness profiles, but none was adequate to fit the data over the full range of r

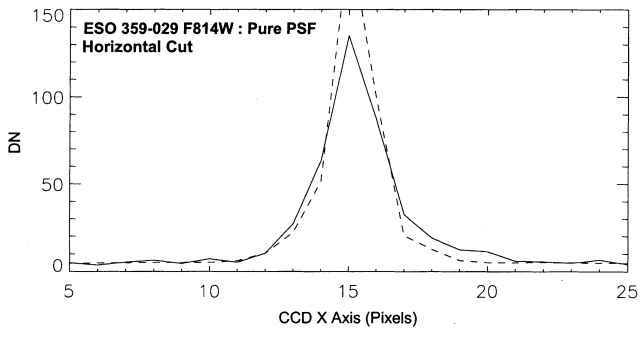

FIG. 2.—Horizontal cut through the ESO 359-029 nucleus in the F814W band (*solid line*) compared with the best-fit Tiny Tim model PSF (*dashed line*). A model PSF scaled to optimize the fit to the wings of the nucleus profile greatly overestimates the central intensity, indicating the nucleus is not a point source and is partially resolved. Axes are counts in DN vs. pixel number, where $x = 15$ represents the center of the extraction box (see text).

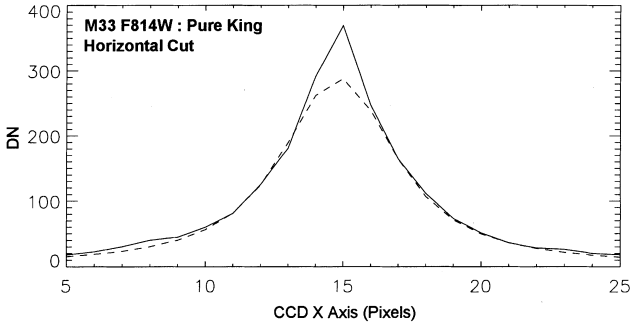

FIG. 3.—Horizontal cut through the M33 nucleus in the F814W band (*solid line*) compared with the best-fit King model (*dashed line*; see text). A King model reasonably reproduces the wings of the nuclear light profile but severely underestimates the central intensity.

for any of the nuclei. In all instances the models severely underestimated the flux in the central regions of the nuclei. Figure 3 shows this is the case even for the best resolved nucleus in our sample, M33.

3.2.3. *Fits Including Extended Components plus a PSF*

To better assess the nature of the light distributions of our nuclei over the full range of r, our final series of modeling attempts consisted of fitting with combinations of a point source and an extended component from Table 3. Our goal was not only to try to reproduce the brightness profiles of each individual nucleus but also to see if we could find a single, unified characterization of all of the nuclei that would allow meaningful comparisons between them. For this reason, we began with our best resolved case, M33.

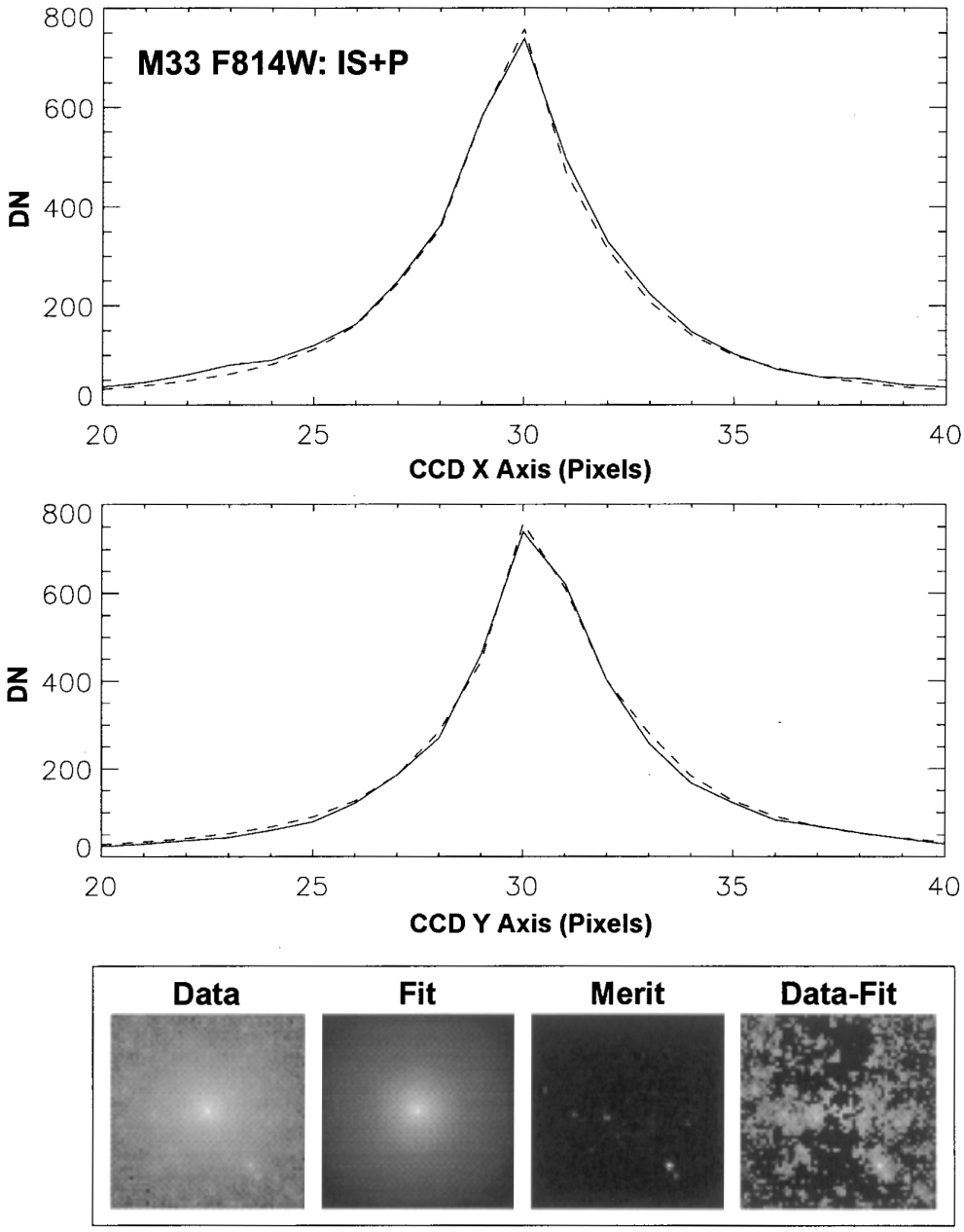

FIG. 4.—Horizontal and vertical cuts through the M33 nucleus in the F814W band (*solid lines*) compared with the best IS + P model fit (*dashed lines*). The four lower panels show 61 × 61 pixel reproductions of the data, the fit, the merit function (see text), and the residuals left after subtraction of the fit from the data, respectively. Solid black areas indicate oversubtraction, and white areas indicate undersubtraction of the observed flux. The structure in the residuals results from the slight elongation of the nucleus compared with the circularly symmetric model. The y-axis has been scaled to a 20 s exposure time.

We first fitted the M33 nucleus in the F814W frame using combinations of a PSF and several of the "classic" brightness distributions given in Table 3. The exponential disk + PSF model fit the wings of the profile adequately but overestimated the peak central brightness. The de Vaucouleurs $R^{1/4}$ law + PSF model was a poor fit for almost the full range of r and significantly overestimated the peak brightness level. The Hubble-Reynolds law + PSF combination roughly fitted the shape of the profile for most values of r but underestimated the peak central intensity. By far, the best fit came from the King law + PSF fit, which provided an excellent model of the brightness profile for all values of r and correctly reproduced the central intensity (Fig. 4). For this model, we found the best fit occurred as $c \rightarrow \infty$—i.e., the best-fit King model tended toward the case of a simple, isothermal sphere (model 9).

Using more generalized fitting formulae with additional free parameters (e.g., models 4, 6, and 8) only marginally improved our fits. One can trade off between γ and the characteristic radii of the models to produce a family of fits, none of them unique (see also KM). In general, the exponent γ becomes larger as the characteristic radius (r'_0, r'_e, or r'_c) increases. Thus while they do reproduce the data adequately, these sorts of generalized fits have no obvious physical meaning and do not permit useful comparisons between the different nuclei. Nonetheless, one important result did emerge: for the modified King model, we found $\gamma \rightarrow 2.0$—i.e., this more general form again tended toward the case of a isothermal sphere. Together, these results suggest that an isothermal sphere is an excellent approximation to the outer brightness distribution of the M33 nucleus, while at *HST* resolutions, the center of the nucleus is indistinguishable from a point source. Because our goal is to fit the observations with a useful and reproducible model rather than exploring all possible model fits (see also KM), we adopt for its simplicity and minimal number of free parameters, the isothermal sphere + PSF (hereafter IS + P) model as an analysis tool for all of our program nuclei.

The emergence of the IS + P model for our program nuclei suggests that *to the resolution limit of our images, the central stellar density continues to increase in all four of our program nuclei.* Although we cannot conclusively rule out other classes of models from our present data (cf. L98), the IS + P model provides a useful and physically motivated characterization of our program nuclei.

Below we present a more detailed analysis of the WFPC2 images of each of our nuclei, including results derived from IS + P model fitting. For each case, we interpret our findings by incorporating results from the present work as well as prior results from the literature.

4. PROPERTIES OF THE TARGET NUCLEI

4.1. *The M33 Nucleus*

Because of the proximity of M33, its very small bulge, and its moderate inclination, its nucleus can be effectively studied from the ground. Spectra by van den Bergh (1976) and Gallagher et al. (1982) and spectral synthesis models of O'Connell (1983) and Schmidt, Bica, & Alloin (1990) show that a range of stellar ages, including stars younger than about 1 Gyr, exist in the nucleus. Massey et al. (1996) deduced from FUV − NUV colors that the young population has a color consistent with a small group of He I emission stars like that seen at the Galactic center. High-resolution ground-based imaging and spectroscopy by KM indicated the nucleus is very compact with a core radius $r_c < 0''.10$ (<0.4 pc), has a stellar velocity dispersion of $\sigma_* = 21 \pm 3$ km s^{-1}, $M/L_V \sim 0.4$, and a maximum central black hole mass of $5 \times 10^4\ M_\odot$.

Despite the lack of a very massive central black hole in the M33 nucleus, there are some indications of mild activity in the form of [N II] optical emission lines (Rubin & Ford 1986), possible short- and long-term optical variability (Lyutyi & Sharov 1990), and a moderately luminous ($\sim 10^{39}$ ergs s^{-1}), variable hard X-ray source (Schulman & Bregman 1995; Dubus et al. 1997). Observations of the center of M33 with the WF/PC-1 on *HST* were presented by Mighell & Rich (1995). They measured a $V-I$ color-magnitude diagram for surrounding field stars that shows a broad red giant branch tip composed of stars with ages ≥ 1.7 Gyr, younger red supergiants, and a main sequence including stars with ages of ~ 0.1 Gyr. We emphasize that M33 cannot be assumed to be simply a massive version of an ordinary globular cluster because its characteristics and environment are much more complex.

The WFPC2 images of the M33 nucleus that we present here were also recently analyzed by L98. These authors found the M33 nucleus to be centrally peaked, which they interpret as a continuous increase in mean stellar density toward a central "cusp." They also noted that the nucleus becomes somewhat bluer in color at small radii. L98 interpret this combination of properties as possibly being due to the presence of binary star merger products in the post–core-collapse nuclear star cluster, as previously suggested by KM. L98 use a deconvolution analysis to derive a fit to the nuclear light profile of M33. Their fit is a steep power-law profile for $0''.05 < r < 0''.2$ with a somewhat shallower central cusp or core with $r_c \approx 0''.034$. They place a further limit on the maximum black hole mass of $M_{\rm BH} < 2 \times 10^4\ M_\odot$ and derive a central luminosity density of $\sim 5 \times 10^6\ L_\odot$ pc^{-3}.

A close inspection of the WFPC2 images of the M33 nucleus reveals several additional interesting features. In agreement with L98, we find the nucleus is clearly elongated, especially in the F555W band, confirming the earlier suggestion of KM. We locate the major axis at a position angle (P.A.) of 18°, in excellent agreement with the value of P.A. = 17° determined by L98.

At a P.A. of roughly −20°, we see evidence of a radial, jetlike feature in both the F555W and the F814W frames (top and bottom panels of Fig. 5, respectively). This feature is roughly 0".5 long and contains two bright knots. In the present data, the structures of these two knots are both consistent with point sources to within errors, but their location, relative orientation, and colors are intriguing. The centroids of both of these bright spots lie along a radial line pointing directly toward the center pixel of the nucleus. The knots have absolute magnitudes (corrected for Galactic extinction) of $M_V = -3.99$ (*top*) and $M_V = -5.21$ (*bottom*), respectively, and there are no other discrete sources of similar luminosity in the outer parts of the nucleus or its surroundings. If these are single stars, they are rather luminous, and it is difficult to explain their highly disparate colors. The upper source is very red [$(V-I)_0 = 1.92$] while the lower source is very blue [$(V-I)_0 = -0.22$] (see Fig. 6, discussed below). Even if the sources we see are luminous stars, their alignment with the nucleus center raises the possibility that they may be associated with a jet or outflow

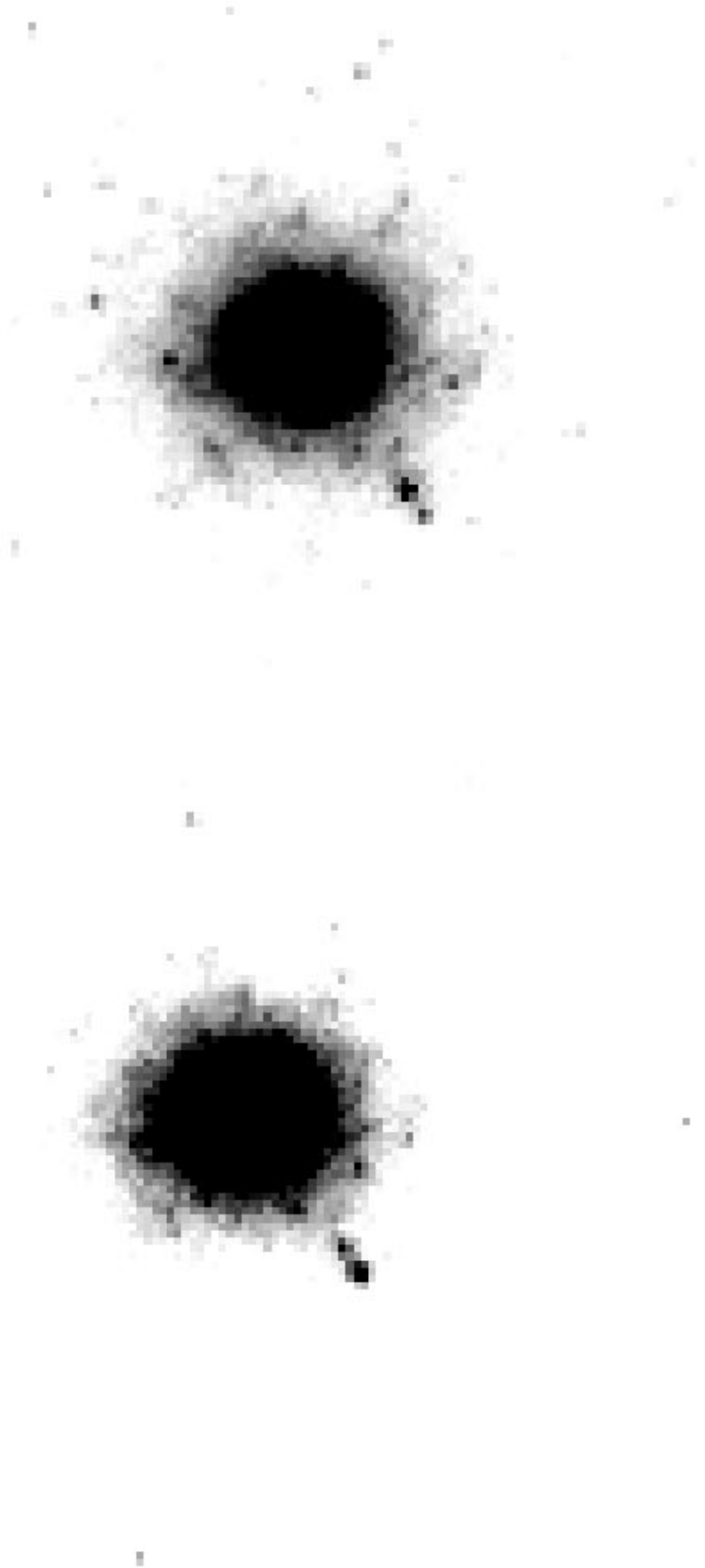

FIG. 5.—Close-ups of the M33 nucleus in the F555W filter (*top*) and the F814W filter (*bottom*). Image sizes are roughly 5″.8 × 5″.8. The gray scales were chosen to emphasize the jetlike feature seen in both wave bands at roughly a "5 o'clock" position. Note that the knots seen in the jetlike structure are significantly brighter than any other features surrounding the nucleus. The lower knot is brightest in the F555W frame, while the upper knot is brightest in the F814W frame. Note also the more pronounced elongation of the nucleus in the F555W image.

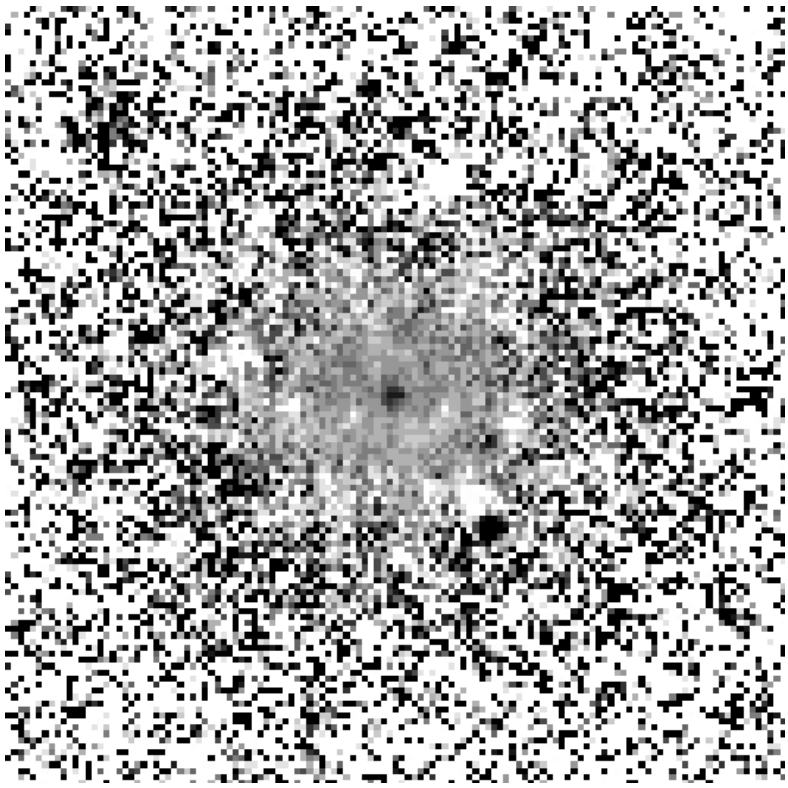

FIG. 6.—F555W − F814W color map of the M33 nucleus. The image is roughly 5″.8 × 5″.8 across. The bluest features are seen as black, and the reddest features appear white. Note the compact blue source at the center of the nucleus [$(V-I)_0 = 0.31$], and the presence of both a very blue source [$(V-I)_0 = -0.22$] and a very red source [$(V-I)_0 = 1.92$] at the position of the jetlike structure seen in Fig. 5. A faint, moderately blue ring is also visible surrounding the periphery of the nucleus. The overall patchy appearance of the color map likely indicates the presence of dust.

of some sort. Further investigation of these features is clearly desirable. If the M33 nucleus does harbor a miniature jet, this would provide evidence that M33 is indeed a low-level AGN.

We attempted fits to the WFPC2 images of the M33 nucleus using our modeling software, as described in § 3.2.3. Our IS + P model reproduces the light profile of the M33 nucleus quite well, aside from small systematic errors due to the slight ellipticity of the nucleus. The mismatch between our circularly symmetric models and the slightly elliptical nucleus of M33 results in a symmetric residual pattern upon subtraction of the model (Figs. 4 and 7). Our derived core radius for the IS component of the M33 nucleus from the F814W image is $r_c = 0''.11$, which is in good agreement with the measurements of KM and Mighell & Rich (1995), both of whom found $r_c \approx 0''.1$. As in the present work, KM also included a central point source to reproduce the compact central source or "cusp" in the brightness profile. Our IS model value for the core radius is an *upper limit* to the physical size of any core in the M33 nucleus. Our value is larger than the slope break radius derived by L98. These authors interpret the unresolved center of the nucleus as a density cusp, the properties of which were measured via deconvolution, while our core radius is derived from an isothermal sphere fit to only the *resolved* portion of the underlying nuclear star cluster. Our resulting IS + P model magnitudes agree well with our aperture photometry (see § 4.7). For example, the observed F555W magnitude for a 25 pixel circular aperture is only 0.01 mag fainter than that derived from our model.

We can derive a limit to the central luminosity density by assuming the flux in the model point source in the unresolved center of the nucleus emanates from a region the size of which is less than 1 PC2 pixel. At the distance of M33, this corresponds to a volume with radius 0.092 pc and the minimum V-band luminosity density for the M33 nucleus of $3.6 \times 10^7\ L_\odot\ \mathrm{pc}^{-3}$. The L98 model yields a lower central density for the M33 nucleus since it assumes a continuous model for the nuclear radial brightness profile.

The color map of the M33 nucleus (Fig. 6) suggests this nucleus has a blue core, as previously inferred by KM, Mighell & Rich (1995), and L98. This result must be interpreted with caution owing to the mismatch between the *HST* PSFs at different wavelengths, but nonetheless, the spatial extent of the blue region on our color map ($\sim$3 pixels) is consistent with the slightly bluer nuclear core measured by L98 in their deconvolved image. From aperture photometry (see below), we measure a $(V-I)_0 = 0.71$ within a 3 pixel radius aperture, also consistent with Figure 21 of L98. If real, this central concentration of blue light could represent a small cluster of young stars (e.g., He I stars, as suggested by Massey et al. 1996), a miniature AGN, or a single blue supergiant. If such discrete sources are present, then the fit of smooth power law to the radial intensity distribution becomes uncertain, as discussed by Sams (1995). Similar behavior is also seen in the Milky Way's nucleus, but in this case it is due to a central concentration of luminous young stars (Krabbe et al. 1995; Mezger et al. 1996). The central young cluster in the Milky Way nucleus would have a core radius of about 0″.03 at the dis-

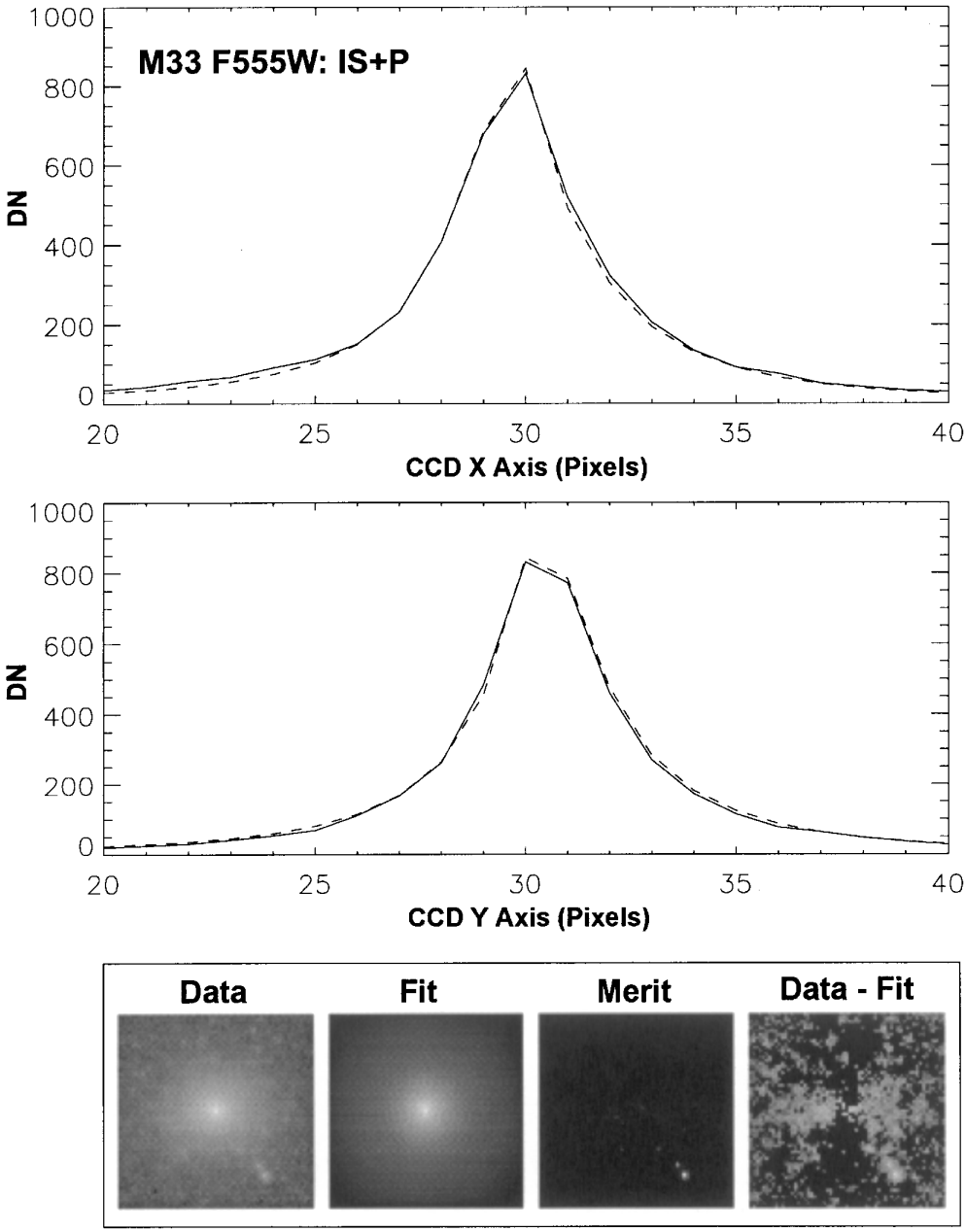

FIG. 7.—Same as Fig. 4, but for the F555W band

tance of M33 and therefore would appear as a blue point source superposed on an older, redder underlying cluster, similar to what we see in M33. We also note that some blue light is present in the outskirts of the M33 nucleus; consistent with the color profile shown in L98, we see a faint, moderately blue ring surrounding the periphery of the entire nucleus (see Fig. 6). It is clear that even low-mass nuclei such as that in M33 are more complicated than simple scaled-up versions of ordinary star clusters, and the radial intensity profile, especially in the central regions, may reflect more than the stellar density profile. Therefore, caution must be exercised in assessing the dynamical state of compact nuclei from brightness profiles alone (see KM; L98).

Because M33 is sufficiently resolved, we can also explore its brightness distribution using isophotal fits. We determined the run of surface brightness with radius for the F555W 20 s exposure using the ELLIPSE task in IRAF. To match the slight elongation of the nucleus, we used a fixed ellipticity of $\epsilon = 0.15$ at a position angle P.A. = 18°. The background was measured in the regions surrounding the nucleus, and a constant background was subtracted. The resulting observed radial brightness profile in the F814W band is shown in Figure 8. For comparison, we also fitted the M33 nuclear brightness profile using circular isophotes. On an azimuthally averaged brightness profile, the results appear virtually indistinguishable from the elliptical fits, indicating the circular symmetry in the IS+P models should not be a major source of uncertainty.

4.2. *The M33-at-a-Distance Nucleus*

Since our other target nuclei are more distant than M33, our WFPC2 observations in these cases suffer more severely from limited angular resolution. However, it is possible to make some comparative measures of the size and radial run of intensity in the outer regions of the other nuclei. This

information provides a basis for testing the hypothesis that other star cluster nuclei in small spirals are structurally similar to the nucleus of M33. It is useful, before undertaking this analysis, to explore first how the observed properties of the M33 nucleus would change if it were moved outside of the Local Group.

As a test of the effects of distance on our model fits, we block-averaged the F814W image of the M33 nucleus by 5×5 pixels to simulate its appearance at a distance of about 4 Mpc (hereafter "M33-at-a-Distance"). The WFPC2 F814W image was selected for this experiment because it is less affected by recent star formation or possible effects of weak nuclear activity and so provides the best measure of the intrinsic properties of the underlying nuclear star cluster. The main source of uncertainty in this experiment comes from the fact that in a real galaxy, an unresolved source would have its flux distributed over the same number of pixels regardless of its distance; however, in our test image, the central point source was binned 5×5.

Our results for the IS+P fits to the M33-at-a-Distance nucleus are presented in Table 4 and Figure 9. These fits demonstrate a few basic points about the impact of resolution on the fitting process. The fraction of the total integrated model flux contained in the PSF increases from 3.4% in M33 to 20% in M33-at-a-Distance. The residuals from the IS+P fit also become much smaller, demonstrating our lessened ability to resolve underlying structure of the nucleus, while at the same time the derived core radius of the extended model component yields a value ~ 1.3 times larger (in parsecs) than for the M33 nucleus at its proper distance. Thus we cannot measure the shape of the central part of distant nuclei without knowing their radial intensity profile in advance.

These effects are to be expected. With increasing distance, more of the light of the nucleus falls within an unresolved point source, and fewer resolution elements lie across the resolved component. As a result, the extended brightness component of the nucleus must be separated from the wings of a strong PSF and cannot be constrained as accurately. Since the PSF also effectively removes additional light from the underlying extended component near the center of the image, the best fitting extended component will necessarily have a shallower brightness gradient at small r. Thus any derived core radius for the IS component of the intensity model will only be an upper limit to the intrinsic r_c.

4.3. *The ESO 359-029 Nucleus*

Sandage & Fomalont (1993) first reported the presence of a pointlike nucleus in ESO 359-029 but classified the host as an Im/dE, N "mixed morphology" galaxy and argued that it is gravitationally bound to the Sbc spiral NGC 1532. However, CCD imaging by Matthews & Gallagher (1997) emphasized the disky appearance of this faint galaxy. They classified ESO 359-029 as an Sd and noted that its disk was small and diffuse, but very symmetric, with a semistellar nucleus centered on an "island" of slightly higher surface brightness than the surrounding disk. In addition, a recent high-resolution H I spectrum by Matthews, van Driel, & Gallagher (1998) shows that ESO 359-029 is clearly rotationally dominated, that the velocity width reported by Sandage & Fomalont (1993) was underestimated, and that the $M_{\rm H\,I}/L_V$ ratio of this galaxy (0.41 in solar units) is entirely normal for extreme late-type spirals, while being a factor of 10 higher than typical dE or dwarf spheroidal systems (e.g., Oosterloo, Da Costa, & Staveley-Smith 1996 and references therein). For these reasons we believe ESO 359-029 is best classified as an extreme late-type spiral of type Sd or Sdm.

We note that ESO 359-029 is physically smaller than the other three galaxies in the present sample and shows almost

TABLE 4

PARAMETERS DERIVED FROM ISOTHERMAL SPHERE PLUS PSF (IS+P) MODEL FITS

	CORE RADIUS[a]								
	F450W		F555W		F814W		% TOTAL FLUX IN PSF		
GALAXY	arcsec	pc	arcsec	pc	arcsec	pc	F450W	F555W	F814W
M33	...	...	0.095	0.40	0.11	0.45	...	5	3
M33-at-a-Distance	...	...	...	...	0.029	0.59	...	...	20
NGC 4242	0.022	0.80	...	...	0.041	1.5	13	...	17
ESO 359-029	0.018	0.88	...	...	0.036	1.8	38	...	25
NGC 4395	0.034	0.43	...	...	0.076	0.96	43	...	48

	$I_{\rm PSF}/I(0)$			$(x_c, y_c)_{\rm PSF} - (x_c, y_c)_{\rm ext}$		
GALAXY	F450W	F555W	F814W	F450W	F555W	F814W
M33	...	0.68	0.64	...	(0.13, 0.17)	(0.32, 0)
M33-at-a-Distance	...	...	1.56	...	...	(0.24, 0.53)
NGC 4242	0.46	...	0.80	(0.66, 0.12)	...	(0.60, 0.04)
ESO 359-029	2.46	...	1.43	(0.01, −0.21)	...	(0.34, 0.19)
NGC 4395	4.0	...	8.5	(−1.17, −0.55)	...	(0.19, 0.01)

NOTES.—Quoted core radii in arcseconds are derived from the best-fitting isothermal sphere plus PSF (IS+P) model fits, as described in the text. Core radii in parsecs are derived using distances from Table 1. The "% Total Flux in PSF" refers to the fraction of the total integrated model flux contained in the Tiny Tim PSF component in each of the respective filters. $I_{\rm PSF}/I(0)$ is the ratio of the peak intensity in the PSF component of the model to the peak intensity of the isothermal sphere component of the model fit; $(x_c, y_c)_{\rm PSF} - (x_c, y_c)_{\rm ext}$ is the relative shift, in pixels, between the centroid of the PSF component of the fit and the extended component of the fit.

[a] All quoted values for the core radii are lower limits (see § 4.2). For the derived range of $I_{\rm PSF}/I(0)$ in the present sample, we estimate maximum uncertainties in our core radius upper limit measurements of $\pm 6\%$ (see § 3.2).

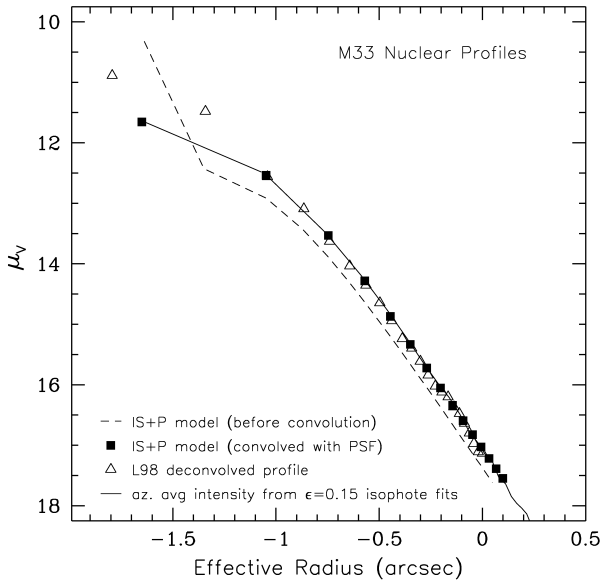

FIG. 8.—Azimuthally averaged representations of the M33 nuclear radial brightness profile in the F555W band. The solid line indicates the observed run of F555W surface brightness (in magnitudes per square arcsecond) as measured through isophotes with $\epsilon = 0.15$ and plotted as a function of effective radius, $r_{\rm eff} = \sqrt{\epsilon a}$, where a is the major axis of the elliptical isophote and ϵ is the ellipticity. The dashed line shows the circularly symmetric IS + P model intensity distribution, before convolution with the PSF, where the central point source is represented as a constant intensity disk with a diameter of 1 pixel. The filled squares show an azimuthal average of the circularly symmetric IS + P model after convolution with the PSF. Note that the effect of PSF convolution in our models is to remove flux from the core and increase the intensity at larger radii. Last, the open triangles show the deconvolved brightness profile derived by L98 (see their Table 5). The excellent agreement between the observed profile measured through elliptical apertures and the circularly symmetric IS + P model shows that our new fit results are not sensitive to small deviations from circular symmetry. In addition, flux is conserved in our IS + P models.

no hint of spiral structure. Like many extreme late-type spirals, its global properties are similar to those of an irregular galaxy (Matthews & Gallagher 1997). This raises the interesting possibility that at least some nucleated dE galaxies may form when gas is stripped from an extreme late-type spiral during a close encounter with another galaxy (cf. Sandage & Fomalont 1993). If extreme late-type spirals were the precursors of dE's, this would eliminate the difficulty of explaining their origins from irregulars, which are generally not nucleated (cf. Binggeli 1994). One way of testing such a scenario is to compare the nuclear properties of galaxies such as ESO 359-029 with those of dE nuclei observed at similar spatial resolutions. One candidate for such a comparison is the Local Group dE galaxy NGC 205. Its nucleus resembles those studied here in terms of its luminosity and size (Jones et al. 1996).

A long-slit spectrum taken by Matthews (1998) revealed that ESO 359-029 has detectable Hα and [N II] emission over most of the optical extent of its disk, but no [S II] was detected. The rotation curve of this galaxy is shallow, slowly rising, and fairly linear, but shows an abrupt reversal near the nucleus, with a semiamplitude of $+25$ km s^{-1} and -13 km s^{-1} on the approaching and receding sides of the nucleus, respectively. Thus, there appears to be a kinematic signature of a compact, massive concentration at the center of this tiny spiral.

The results from IS + P model fits to the ESO 359-029 nucleus are presented in Table 4 and Figures 10 and 11. ESO 359-029 is satisfactorily fitted in both the F450W and the F814W bands by the IS + P model. We see only a very weak, slightly elongated residual in the F814W frame and essentially no discernible residuals in the F450W fit. The core radii we derive for the resolved component of the ESO 359-029 nucleus from our IS + P model fits are the largest of the four galaxies in our sample, although ESO 359-029 is also the most distant of the four and we emphasize our r_c values are only upper limits (see § 4.2). In the blue band 38% of the model flux lies in the point-source component of the fit, suggesting we have only marginally resolved this nucleus. In a manner similar to the case of M33, we derive a minimum central B-band luminosity density for ESO 359-029 from our IS + P model of $2.9 \times 10^4\ L_\odot\ {\rm pc}^{-3}$ within a volume of radius 1.10 pc. Finally, we note that in spite of its faintness (and hence seemingly comparatively low mass), the nucleus of ESO 359-029 is clearly very compact. The nucleus of ESO 359-029 appears to share basic similarities in its properties with the other compact star cluster nuclei in our sample, hinting that the properties of compact star cluster nuclei are at least to some degree independent of the size and luminosity of their host galaxies.

4.4. *The NGC 4242 Nucleus*

In the atlas of Sandage & Bedke (1994), the morphological appearance of NGC 4242 is very similar to that of NGC 4395. Van den Bergh (1995) drew attention of the prominent semistellar nucleus visible in that image. However, unlike the case of NGC 4395, there are no spectral signatures of activity in this nucleus. Ho et al. (1995a) published an optical spectrum of the NGC 4242 nucleus showing weak emission lines, and Heckman (1980) failed to detect a compact nuclear radio source down to a limit $\log (L_{6\rm cm}) < 18.91$ W Hz^{-1}. The lack of discernible far-IR emission from this nearby spiral by *IRAS* and its relatively weak global radio continuum flux (Gioia & Fabbiano 1987) both suggest a low rate of global star formation throughout the disk.

Visual inspection of our images of the nucleus of NGC 4242 (e.g., Fig. 1) reveals very faint, extended "fuzz" around the main bright nucleus. This is most evident in the F814W image. Results from IS + P model fitting are presented in Table 4 and Figures 12 and 13. From this model we derive a minimum B-band central luminosity density for this nucleus of $1.0 \times 10^5\ L_\odot\ {\rm pc}^{-3}$ within a volume of radius 0.815 pc. We find the NGC 4242 nucleus is unlike the other nuclei in our sample in two important ways. First, this is the only one of the four nuclei that shows more structure in the F814W images than in the F450W image. Our IS + P model provides a good fit to the F450W brightness distribution, but in the F814W band, this model cannot properly reproduce the flux distribution in the central few pixels and leaves an oval-shaped residual pattern roughly $0\farcs5 \times 0\farcs3$ across (see Fig. 13). This reveals that this nucleus in not circularly symmetric and that it appears to contain a miniature barlike feature near its center. We see marginal evidence for a similar feature in the F814W image of ESO 359-029, but it is significantly less pronounced. This may be due to an intrinsic difference or to the poorer spatial resolution in the ESO 359-029 images. The second difference between NGC 4242 and the other nuclei is that NGC 4242 is the only one of the three nonactive nuclei where the point source contri-

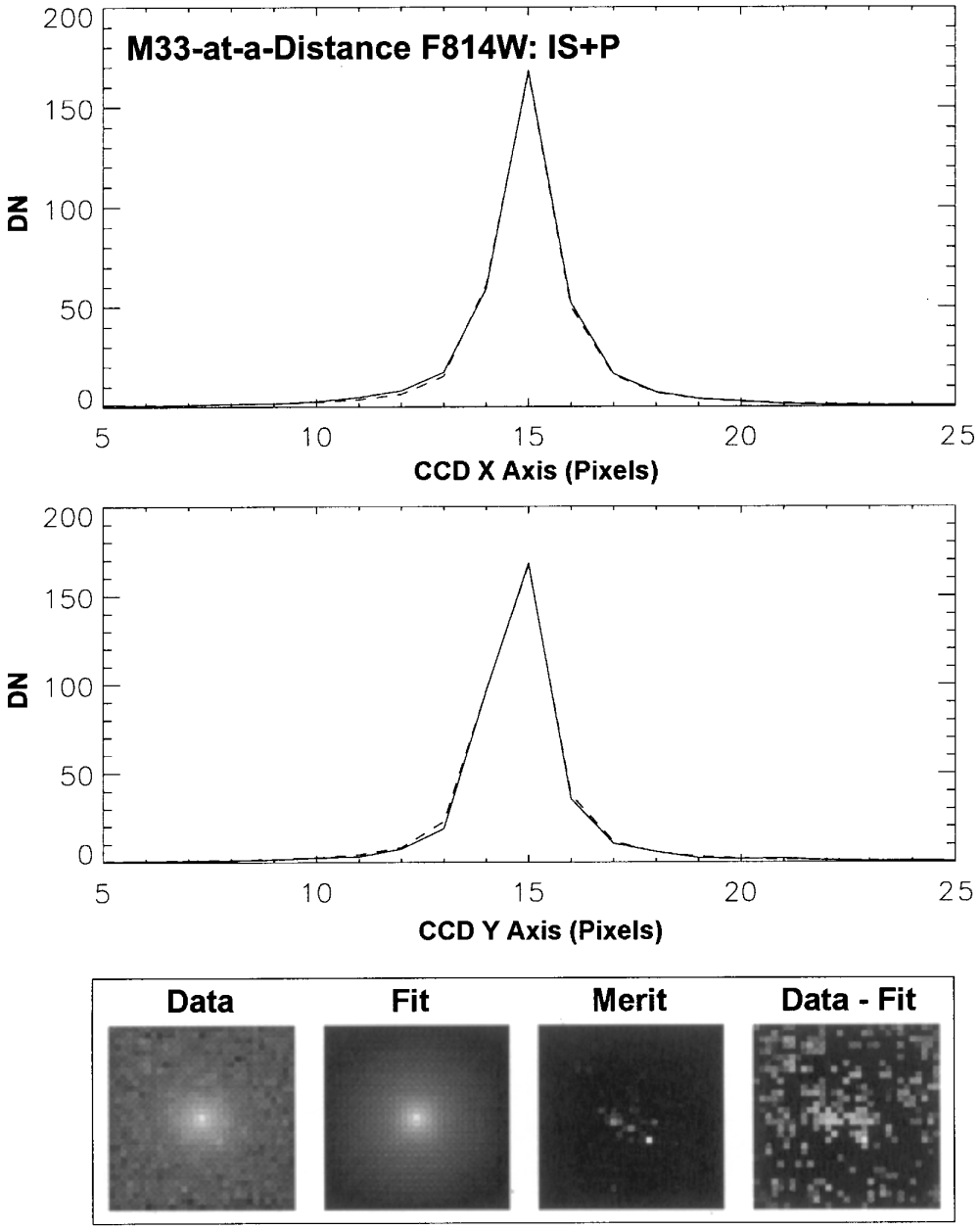

FIG. 9.—Horizontal and vertical cuts through the M33-at-a-Distance nucleus in the F814W band (*solid lines*) compared with the best IS + P model fit (*dashed lines*). The four lower panels are the same as in Fig. 4, except that the images sizes are 31 × 31 pixels. Note that the residuals are less significant than for M33 (Figs. 4 and 7).

bution to our model fits is larger in F814W than in the bluer image.

4.5. *The NGC 4395 Nucleus*

Filippenko & Sargent (1989) were the first to present evidence that the compact nucleus of NGC 4395 is the lowest luminosity Seyfert 1 known. These authors discovered that the Hα emission line in the NGC 4395 nucleus has a broad component, and that the [O III] emission is much stronger than that of Hβ. Further support for the presence of an AGN came from a UV spectrum taken with the Faint Object Spectrograph on *HST* by Filippenko et al. (1993), which showed a flat far-UV continuum with strong, high ionization emission lines. No P Cygni profiles were found in the UV, such as would normally be present from winds in massive OB stars. In addition, Filippenko et al. found the nucleus to be spatially extended in observations made with the original Planetary Camera through the F502N filter (a narrowband O III filter), while the continuum F547M filter showed only a point source. Sramek (1992) measured a nonthermal radio source with about the luminosity of the Cas A Galactic supernova remnant at the position of the NGC 4395 nucleus. Finally, Lira & Lawrence (1998) have recently reported the nucleus is a variable X-ray source. Taken together, the spectral characteristics of the NGC 4395 nucleus appear to be more consistent with a standard accretion-powered AGN rather than a compact starburst.

With our new WFPC2 data, we have resolved the nucleus of NGC 4395. This nucleus has complex internal structure.

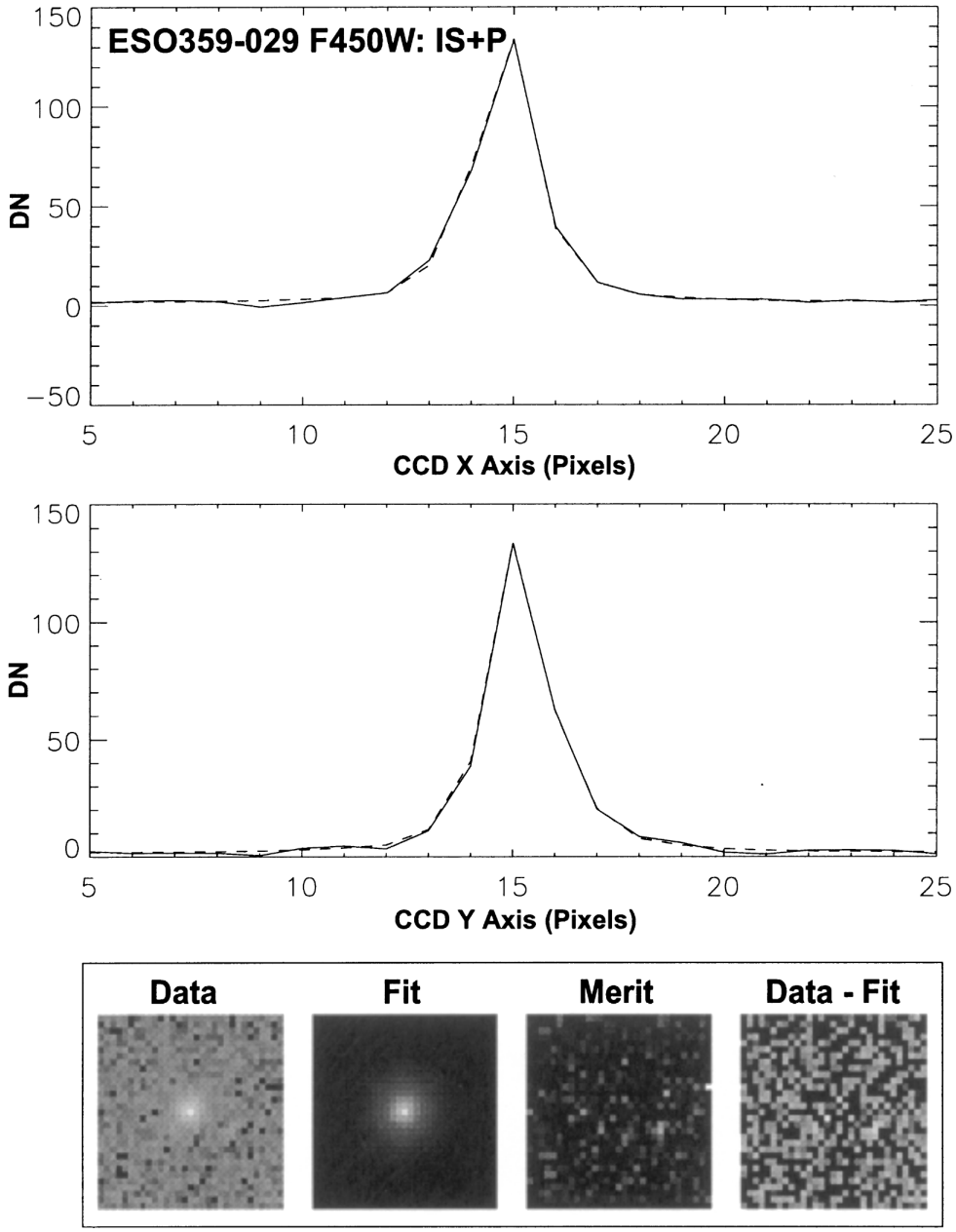

FIG. 10.—Horizontal and vertical cuts through the ESO 359-029 nucleus in the F450W band (*solid lines*) compared with the best IS + P model fit (*dashed lines*). The four lower panels are the same as in Fig. 9.

In both the F450W and F814W bands, some degree of elongation is visible, and a faint halo of irregular "fuzz" can be seen surrounding the brighter core of the nucleus.

Because the NGC 4395 nucleus is less structurally complex in the F814W frame, we modeled that image first. The resolution of the nucleus in F814W is illustrated in Figure 14, where we have subtracted a scaled PSF model to approximately fit the central intensity. This leaves behind an extended, slightly elliptical residual pattern that contains about half of the light. A complete fit to the nucleus can be made with good accuracy using our IS + P model (Fig. 15); this produces a point source and extended object centered at the same position to within better than 0.1 of a PC2 pixel ($\approx$5 mas). As with our other sample nuclei, the outer regions of the nucleus of NGC 4395 are reasonably fitted by an IS + P model. However, for NGC 4395 an asymmetric, bipolar-like pattern emerges in the residuals (Fig. 15). The luminosity of the IS component of NGC 4395's nucleus in the I band is $M_I \approx -10.1$ (see § 4.7), similar to the resolved nuclear cluster components in the other galaxies in our sample. The luminosity and structural parameters of the NGC 4395 nucleus that we measure from the present data are consistent with NGC 4395 containing a normal star cluster nucleus which is currently hosting nuclear activity. However, final confirmation of this picture will require high angular resolution spectra.

The NGC 4395 nucleus looks considerably different in the F450W filter. Two of the central pixels of the F450W image were saturated in the long exposure; hence these were replaced by values derived by scaling from our short exposure (see § 2).

Visually inspecting the F450W image, we see that the nucleus of NGC 4395 is asymmetric and elongated (Fig. 16); it can be described as a point source superimposed on an

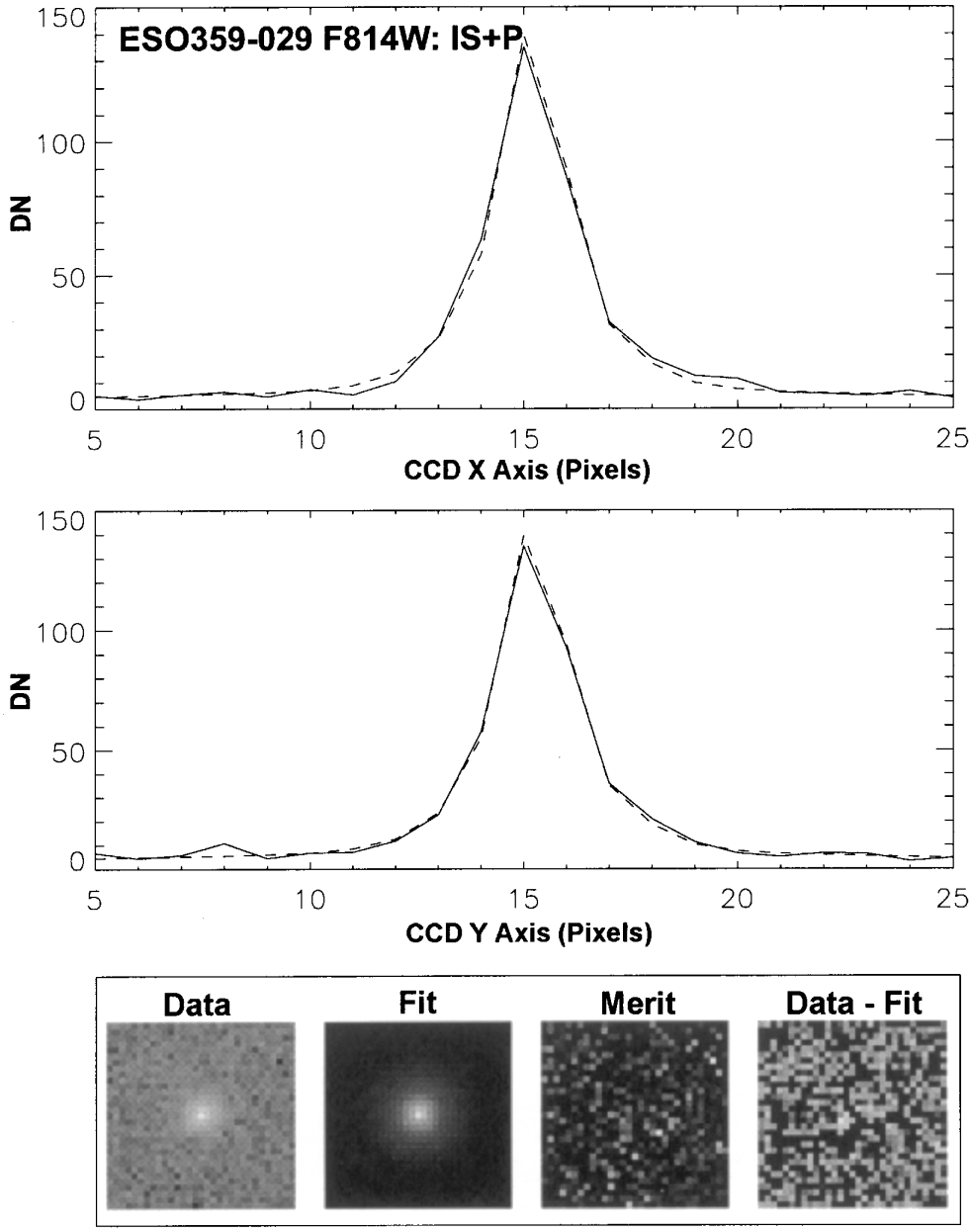

FIG. 11.—Same as Fig. 10, but for the F814W filter

elongated, somewhat irregular structure. We have selected the contour levels in Figure 16 to attempt to illustrate this point; note the displacement of the center from the outermost isophote. Furthermore, unlike the other nuclei, where the centers of the PSF and IS components to the fits coincide to within a fraction of a pixel (see Table 4), the centroids of the PSF and IS components for the F450W image of NGC 4395 are offset by 1.2 pixels, and the centroid of the IS component differs from that found in the F814W image by nearly 2 pixels. The luminosity in the point-source component is considerably higher than would be expected from the effects of distance alone (based on our M33-at-a-Distance experiment), arguing that this nucleus truly contains a very compact source near its center, consistent with other AGNs. A fit to the light distribution in the F450W frame using our IS+P model leaves a bipolar residual pattern similar to that in the F814W frame, but much more pronounced and containing an even larger fraction of the total nuclear light (Fig. 17). From our IS+P model we place a limit on the minimum B-band luminosity density in the NGC 4395 nucleus of $9.6 \times 10^6\ L_\odot\ \mathrm{pc}^{-3}$ within a volume of radius 0.283 pc.

Further hints of the complex structure of the NGC 4395 nucleus can be gleaned from an examination of a F450W−F814W color map (Fig. 18). We see overall the nucleus is fairly blue, with a compact central source that appears to be somewhat bluer than the surrounding regions. There is also a short, bright blue arc ($\sim$0.″4 long) offset just a few pixels from the nucleus center. This and the prominent extended blue plume visible to the right of the nucleus are discussed in detail below.

As with the F814W frame, we examine the residuals left after subtracting only the point source component of our model (Fig. 19). From this, we see evidence of a slight elongation at a P.A. = 255° (at "2 o'clock") in the F450W image. No analogous feature was seen in the F814W image

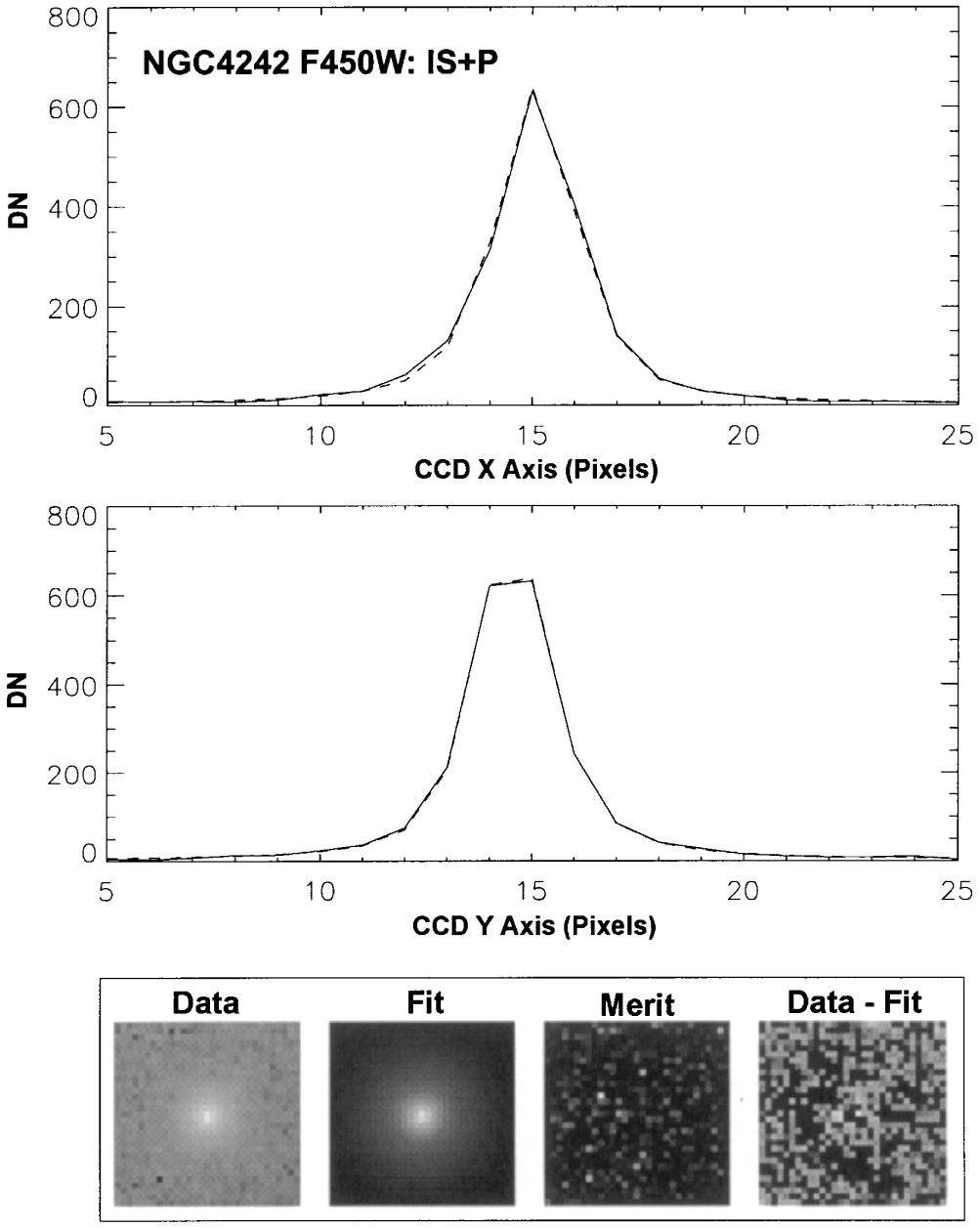

FIG. 12.—Horizontal and vertical cuts through the NGC 4242 nucleus in the F450W band (*solid lines*) compared with the best IS + P model fit (*dashed lines*). The four lower panels are the same as in Fig. 9.

(Fig. 14). The elongated structure is only weakly visible, but if the feature were simply an artifact of an error in the PSF, we would expect to see a reflected symmetry in this structure, and we do not. The stronger evidence of the reality of these features is that it appears to correspond to a feature in our contour plot (Fig. 16) and to a distinct blue arc in the color map shown in Figure 18. In the color map, the arclike feature is located about 0.″25 ($\sim$3 pc) from the center of the nucleus. The structure of this arc and its extremely blue color are consistent with it being produced by emission lines from ionized gas (see below).

These asymmetric blue structures we see in the NGC 4395 nucleus are most readily understood if the light is due to gas rather than stellar emission; dynamical timescales within nuclei are extremely short, and thus any azimuthal irregularities in the distributions of stars will rapidly disappear in much less than 1 Myr. A stronger confirmation of this picture comes from the consistency of our observed asymmetry in the NGC 4395 nucleus with that found by Filippenko et al. (1993) in their F502N-band observations. This agreement suggests that the inner and outer filaments are due to regions where the Hβ and [O III] emission lines are especially intense. Using the WFPC2 efficiencies tabulated by Biretta et al. (1996), we find that the blue arclike feature produces a flux in [O III] of $\sim 4.5 \times 10^{-14}$ ergs s^{-1} cm^{-2}, which is about one-fourth to one-third of the [O III] flux measured from ground-based spectra by Ho et al. (1997a), and corresponds to a luminosity of roughly 1×10^4 $L_\odot$.

The F450W image of NGC 4395 contains a second, large emission plume that is clearly resolved from the main nucleus (Fig. 20). It is approximately aligned with the inner blue arc discussed above. This plume also has the blue colors expected for an emission-line source and is only

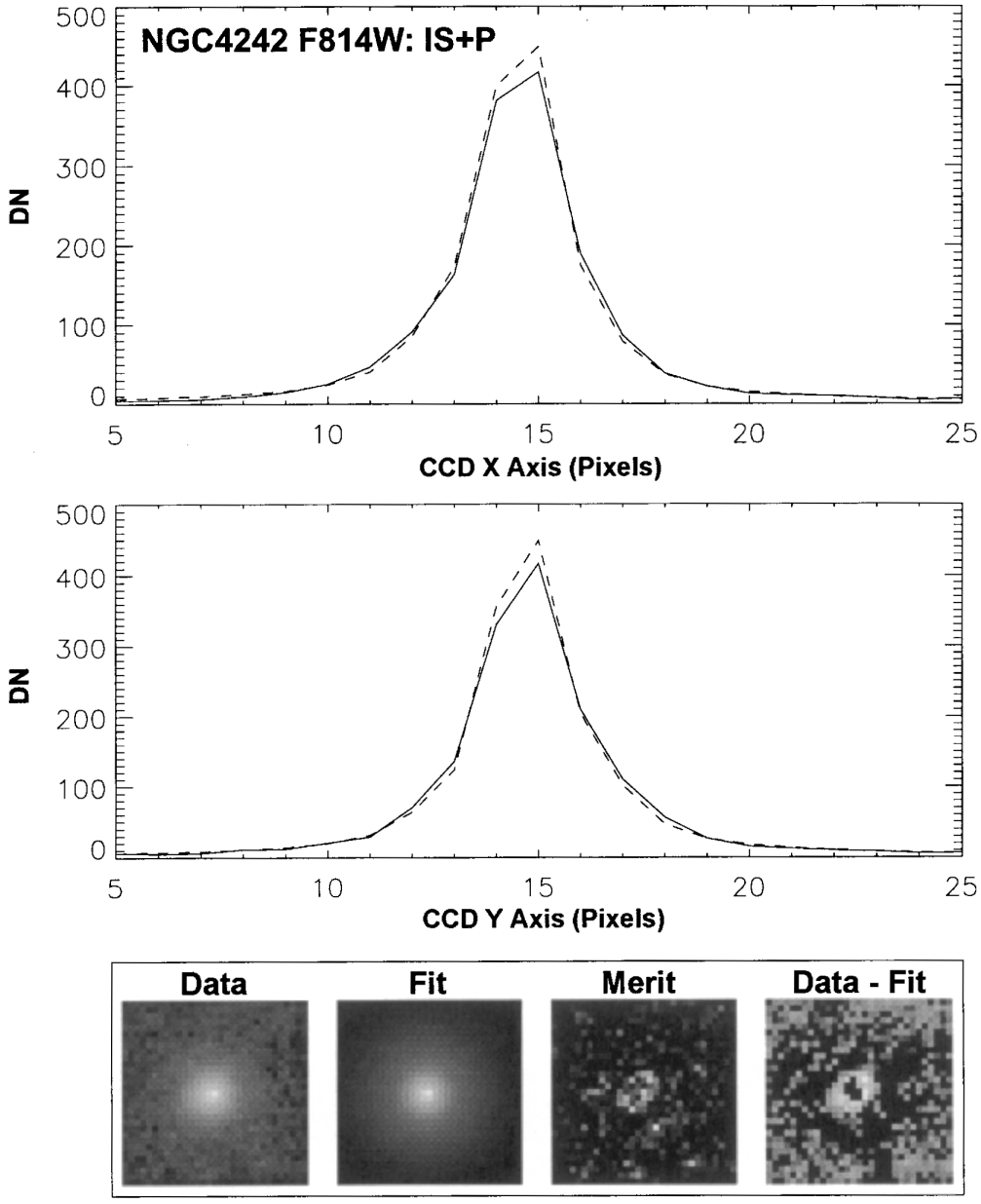

FIG. 13.—Same as Fig. 12, but for the F814W filter. Note the prominent bar-shaped structure visible in the residuals.

faintly visible in the F814W image (Fig. 1). The outer plume has a wispy, filamentary structure and extends about 1″ (~20 pc) in projected distance from the nucleus, with its main structure centered near P.A. = 265°. Near P.A. = 270°, it makes a 90° turn and joins onto a fainter region at P.A. = 280°. We detected an integrated flux from the outer plume is 44 photons s^{-1}, corresponding to corresponding to a flux in [O III] of 4×10^{-14} ergs s^{-1} cm^{-2}, or $L(\mathrm{O\ III}) \geq 1.5 \times 10^{38}$ ergs $s^{-1} \approx 1 \times 10^4\ L_\odot$. Thus, this emission-line plume, together with the arc discussed above, contains one-half to two-thirds of the [O III] flux found by Ho et al. (1997a) in their spectra taken with a 1″ × 4″ entrance aperture. Since Ho et al. (1997a) quote an uncertainty of ±20% for their measurement, our values are in rough agreement. We therefore believe that these two features comprise the bulk of the narrow emission line region around the Seyfert nucleus of NGC 4395.

Our observations of the structure and luminosity of the NGC 4395 nucleus and its surroundings are consistent with the behavior of more luminous AGNs. Normal Seyfert galaxies often show "ionization cones" along which highly ionized material is found (e.g., Pogge 1989a, 1989b; Wilson et al. 1993; Boksenberg et al. 1995; Mulchaey, Wilson, & Tsvetanov 1996; Schmitt & Kinney 1996). This phenomenon is interpreted as blocking or collimation of radiation from the vicinity of an accreting black hole. The presence of two distinct filaments along approximately the same position angle from the nucleus gives strong evidence for the presence of an ionization cone in NGC 4395. This feature, in combination with the spectrum and brightness of the probable [O III] line emission, provide further support to the presence of an AGN within the central parsec of the NGC 4395 star cluster nucleus. These factors strengthen arguments against a stellar origin (e.g., the "Warmer"

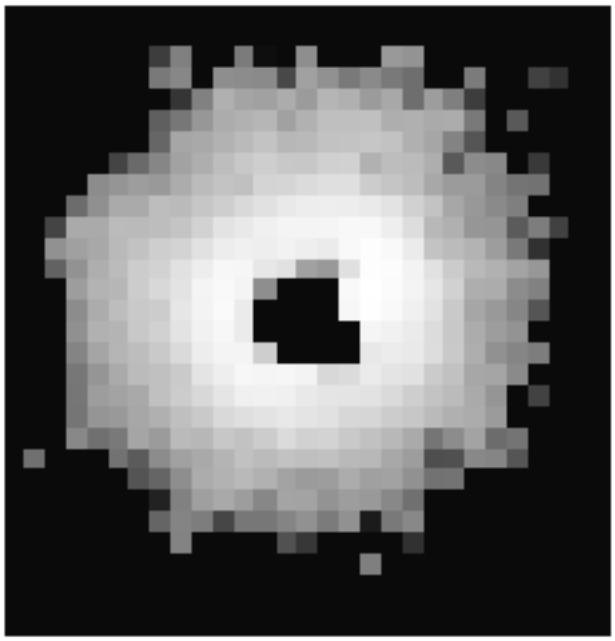

FIG. 14.—A 31 × 31 pixel image showing the residuals after subtraction of the best-fitting PSF from the NGC 4395 nucleus in the F814W image. Note the slight elongation of the residuals, which contain roughly half the total nuclear flux.

model of Terlevich & Melnick 1985) for the activity in NGC 4395 (see also Filippenko et al. 1993).

4.6. *Comparison of the Structural Properties of the Nuclear Star Clusters*

The emergence of the isothermal sphere as a suitable approximate model for the outer brightness profiles of our nuclei suggests that the nuclei of all of our sample galaxies harbor true compact nuclear star clusters, not simply small, nuclear H II regions. In contrast to the isothermal sphere, the more general King law (King 1962, 1966) includes a finite value for the cutoff or "tidal" radius r_t (see eq. [5], Table 3). What does it mean then that our present nuclei are better fitted as $r_t \to \infty$ (or equivalently, $c \to \infty$) than with the more general King law? One possibility is that we are unable to measure r_t owing to our limited field of view and confusion from the background light of the galaxy. However, in the center of a rigidly rotating galaxy, the tidal radius loses its usual physical interpretation, and the nucleus may simply blend into the disk, as discussed by KM. The result would then be a very slow drop-off in stellar density from a nuclear star cluster in galaxies with shallow central gravitational potentials; stars will become unbound from the cluster only at radii at which the effects of galactic rotation begin to dominate.

A comparison of the properties we derive for our sample nuclei from IS+P model fitting reveals both some interesting similarities and some important differences. The fit results yield two cases (M33 and ESO 359-029) where a larger percentage of the integrated model fluxes lie in the point-source component at bluer wavelengths. Since the intrinsic resolution is slightly better at shorter (bluer) wavelengths, this may reflect a real, underlying property of these nuclei—i.e., that they contain a compact, blue central source (or possibly a blue "cusp").

In comparing the core radii we derive for the IS component of each of our nuclei (Table 4), we see some expected effects of distance. As predicted from our test fits to M33-at-a-Distance, the fraction of the total flux in the central PSF increases from M33 to NGC 4242 at a distance of 7.5 Mpc and again for ESO 359-029 at 10.2 Mpc. If the overestimation of the core radius that we measured for M33-at-a-Distance can be assumed to scale roughly linearly with distance, we estimate that the star cluster components of all four of our sample nuclei have similar sizes. Despite the uncertainties, we note that the nuclei for which we have both F450W and F814W data, our derived core radii from the IS+P models are all $\sim$2 times larger in the F814W images than in F450W. This result is independent of the differing fraction of the flux in the PSF component in the different galaxies. This provides a tantalizing hint that our inactive nuclei have underlying structural similarities—i.e., an outlying population of old or intermediate-age red stars dominating the light at larger radii, and an increased blue luminosity contribution toward the center. This type of segregation is found in the Milky Way nuclear star cluster, although in the Milky Way nucleus the core radius of the older, red stars is $\sim$5–10 times that of the inner blue population (see Eckart et al. 1993; Rieke & Rieke 1994; Krabbe et al. 1995). Alternatively, blue nuclear cores could result from dynamical processes, such as enhanced binary production leading to excess populations of blue straggler stars (KM; L98), or ultra–low-luminosity AGNs.

4.7. *Aperture Photometry of the Nuclei*

We established in § 4 that none of our program nuclei are fully resolved. Only the nucleus of M33, which can be traced over a diameter of about 7″ (28 pc), comfortably exceeds the size of our model of the WFPC2 PSF. However, in all cases the nuclei stand out from their surroundings on the WFPC2 images (§ 5), and thus aperture photometry is relatively straightforward. This is a major advantage of *HST* data, which typically offer at least 10 times greater angular resolution than optical observations from the ground.

Aperture photometry was carried out using standard software packages in IRAF. We selected aperture sizes to include approximately 90% of the light from each nucleus. For the M33 nucleus, we used radii of 50, 75, and 85 pixels (diameters of 4.″6, 6.″9, and 7.″8), 30 pixels radius (diameter of 2.″76) for NGC 4242 and NGC 4395, and 20 pixels radius (diameter of 1.″84) for ESO 359-029. Images were background-subtracted prior to photometering using background measures obtained from regions adjacent to the nucleus. Because our galaxies all lack bulges, the disk background light was comparatively weak relative to the nucleus. We derived magnitudes in the WFPC2 system as described in Holtzman et al. (1995b). These are given for each WFPC2 filter i_λ by

$$m(i_\lambda) = -2.5 \log (\mathrm{DN\ s^{-1}}) + 0.748 + \mathrm{ZP}[m(i_\lambda)] \quad (1)$$

for observations made with GAIN = 7. DN is the data number, and the filter zero points, ZP$[m(i_\lambda)]$, are given in Table 9 of Holtzman et al. (1995b). We adopted observed zero points for the F555W and F814W filters and the synthetic zero point for F450W.[16] The resulting WFPC2 instrumental magnitudes for M33 were converted to *VI*

[16] Technically, magnitudes on the WFPC2 system are defined for a point source observed through a 0.″5 aperture; there is no standard convention for adapting this system to extended sources.

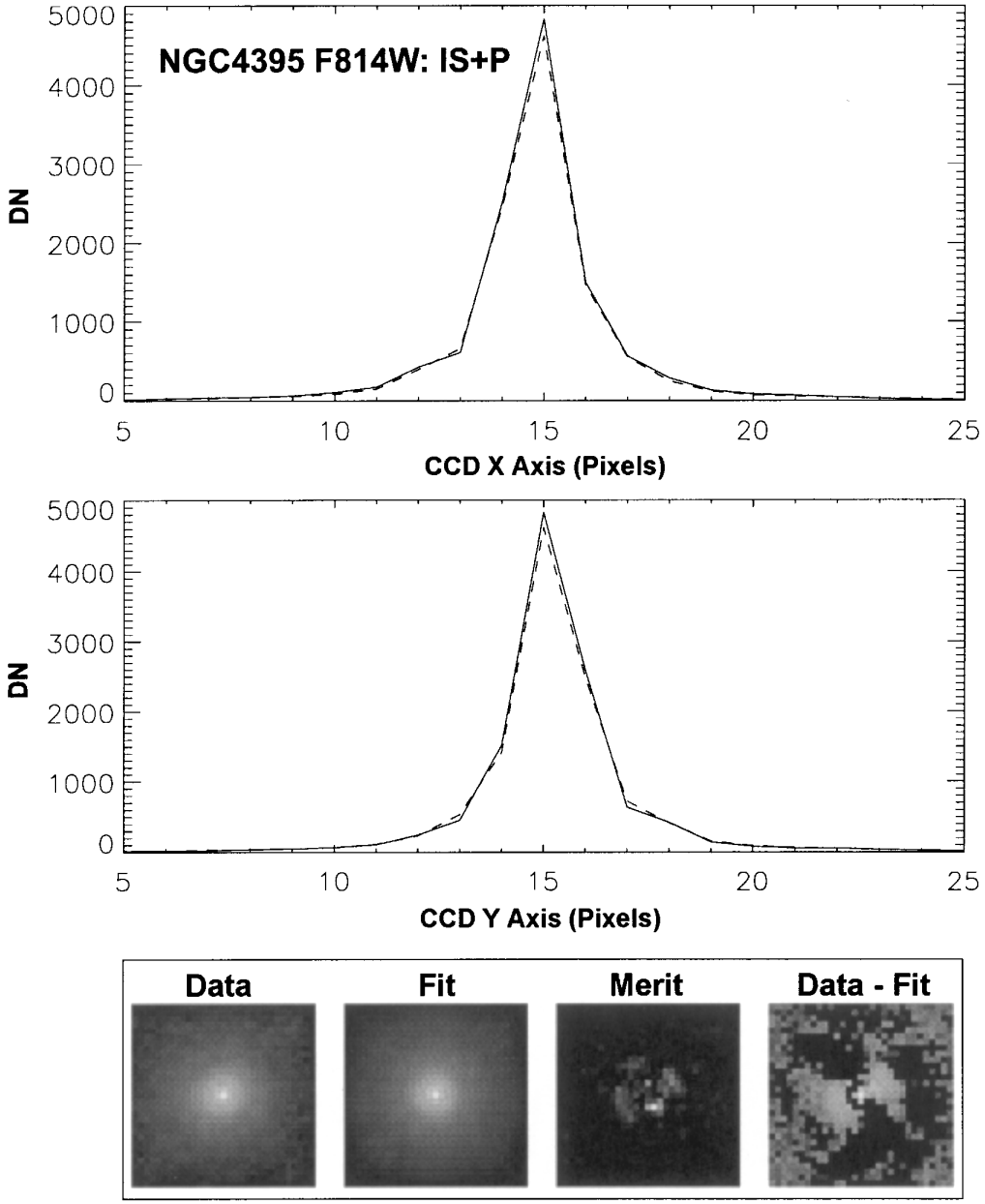

FIG. 15.—Horizontal and vertical cuts through the NGC 4395 nucleus in the F814W band (*solid lines*) compared with the best IS + P model fit (*dashed lines*). The four lower panels are the same as in Fig. 9. Note the bipolar pattern in the residuals.

magnitudes following Holtzman et al. (1995b), while those of the other galaxies were transformed to the *BI* system using new relationships derived by J. A. Holtzman (1998, private communication):

$$I = \begin{cases} m_{\rm F814W} - 0.002(B-I) - 0.009(B-I)^2, \\ \qquad\qquad \text{if } B-I < 1.3\ , \\ m_{\rm F814W} - 0.004(B-I) - 0.003(B-I)^2, \\ \qquad\qquad \text{if } 1.3 < (B-I) < 3; \end{cases}$$

$$B = \begin{cases} m_{\rm F450W} + 0.108(B-I) - 0.008(B-I)^2, \\ \qquad\qquad \text{if } B-I < 1.3\ , \\ m_{\rm F450W} + 0.315(B-I) - 0.047(B-I)^2, \\ \qquad\qquad \text{if } 1.3 < B-I < 3.0\ . \end{cases}$$

Here $m_{\rm F814W}$ and $m_{\rm F450W}$ refer to the WFPC2 system magnitudes given by equation (1). Our B and I magnitudes are presented in Table 5.

Past ground-based measurements can be used to check our results for the M33 nucleus. Photometry by Nieto & Aurière (1982) and by KM yielded $B = 14.5 \pm 0.1$ and $B = 14.57 \pm 0.07$, respectively. Combining our observed value of $V = 13.80 \pm 0.05$ with $B-V = 0.68$ measured by Walker (1964), we find excellent agreement between our new WFPC2 photometry and ground-based measurements, as well as with the WFPC2 measurements of L98. Our V magnitude also agrees within errors with the value of $V = 13.82$ measured by Sharov & Lyutyi (1988).

Absolute magnitudes in Table 5 are derived from the distances and extinction values given in Table 1. Our sample is not large enough to explore adequately possible correlations between host galaxy luminosity and the luminosity of the nuclei, although we do find the most luminous nucleus (that of M33) in the most luminous host galaxy and the least luminous nucleus (that of ESO 359-029) in the intrinsically faintest host galaxy. However, what is perhaps

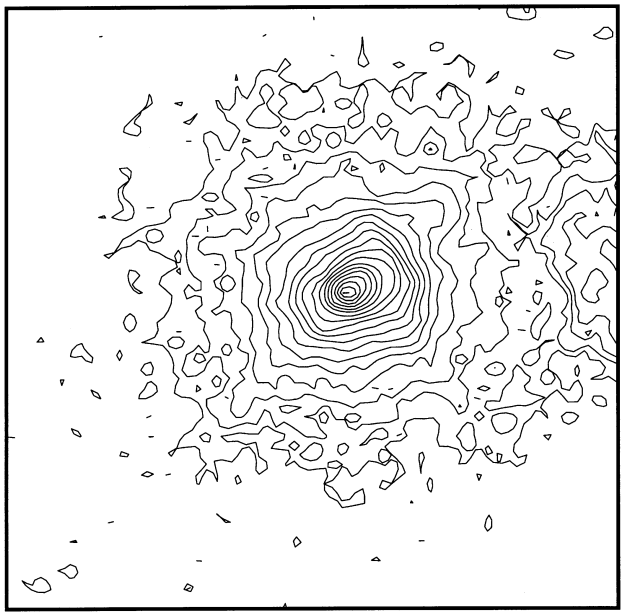

FIG. 16.—Contour plot of the NGC 4395 nucleus in the F450W filter. The field size is 64 × 64 pixels. The contours are spaced at 0.5 mag intervals. The peak surface brightness corresponds to $\mu_{F814W} \approx 13.3$ mag arcsec^{-2}. Note the elongation of the nucleus and the displacement of the central point source from the outermost isophotes.

more intriguing is the *similarity* of the luminosities ($M_I \sim -11 \pm 1$) of all of the nuclei in spite of the range in luminosities of their host galaxies from $M_V = -15.1$ to $M_V = -18.2$. This demonstrates that nuclei of similar luminosities can be either active or nonactive and raises the possibility that the nuclei share similar origins and long term evolutionary histories.

In spite of the fairly small range in luminosities of our target nuclei, the spread in their colors is significant. Interestingly, M33, while having the reddest nucleus in our sample, has the bluest nucleus in the Local Group (Sharov & Lyutyi 1988). NGC 4242 and ESO 359-029 have intermediate colors, both somewhat bluer than typical globular clusters. Finally, the active nucleus in NGC 4395 stands out because of its extremely blue optical colors, making it nearly as luminous as the M33 nucleus in the blue. These blue colors argue against the suggestion of Carollo et al. (1997) that faint nuclear star clusters in quiescent disk galaxies are old stellar clusters, but rather hints that they could contain a mixture of stellar ages. Alternatively, binary mergers in old star cluster nuclei could yield a range in optical colors (see L98), as could the presence of low-luminosity AGNs. Spectroscopy and spectral synthesis studies will be needed to better explore this issue. Such studies may also yield clues as to why a spread of nearly 1 magnitude in $B-I$ exists among the three nonactive nuclei in our sample. One possible explanation for the observed color spread is that episodic star formation occurs in these types of nuclei (e.g., Firmani & Tutukov 1994). All three galaxies have similar inclinations ($i \sim 50°$), so reddening from extinction in the surrounding galactic disks is unlikely to contribute much to this spread.

TABLE 5

WFPC2 PHOTOMETRY OF NUCLEI

Filter	M33	ESO 359-029	NGC 4242	NGC 4395
m_{F450W}	...	21.40	19.47	16.77
m_{F555W}	13.83	...	...	...
m_{F814W}	12.86	20.18	18.84	16.90
m_I	12.83	20.17	18.78	16.93
$V-I$.....	0.88	...	...	...
$B-I$.....	1.49[a]	1.38	0.71	−0.16
M_B	−10.4	−8.5	−9.8	−10.3
M_I	−11.9	−9.9	−10.5	−10.2

NOTES.—Here m_{F450W}, m_{F555W}, and m_{F814W} are the observed apparent magnitudes in the WFPC2 magnitude system described by Holtzman et al. 1995b; m_I is the apparent magnitude, converted to I band. Transformations to the VI and BI systems were made following Holtzman et al. 1995b and J. A. Holtzman (1998, private communication), respectively, and then corrected for Galactic reddening. Adopted distances and extinctions are presented in Table 1. Further details of the photometry are described in the text.

[a] The M33 B magnitude was derived from the WFPC2 F555W magnitude and the ground-based $B-V$ color from Walker 1964.

5. ENVIRONMENTS OF THE NUCLEI

A striking characteristics of the nuclei in our sample is the visual appearance of each relative to its respective surrounding galactic disk. In all cases, the nuclei are "naked"—i.e., they appear very distinct from their circumnuclear environment, and there is little evidence for significant quantities of dust or other material at the centers of these galaxies (see Fig. 1). While, to some extent, the nuclei in the present sample were selected on this basis, we have confirmed that this holds even at space-based resolutions. These nuclei thus represent density contrasts of roughly 1000:1 compared with their surroundings. This point becomes especially evident in the F814W image of NGC 4395, where what appear to be two background galaxies can be seen through the disk, only tens of parsecs from the nucleus (Fig. 21; for contrast with luminous spirals, see the collection of *HST* nuclear region images of Carollo et al. 1997). Furthermore, for all of our sample galaxies, the continuum light from the galaxy disk is only weakly detected during the WFPC2 exposures, and we see no hints of spiral structure. While all the disks are actively forming stars, as evidenced by the presence of Hα emission, there is little central concentration of star formation in any of the galaxies (e.g., Wang, Heckman, & Lehnert 1997; J. S. Gallagher & L. D. Matthews 1993, unpublished). These properties of the nuclear regions of our sample galaxies set their nuclei apart from those in most other well-studied nearby spirals where the nuclei occur within an obvious bulge component, or lie at the center of a spiral pattern (e.g., Pişmiş 1987 and references therein; Carollo et al. 1997; Regan & Mulchaey 1998), and where significant quantities of molecular gas and dust exist in the inner regions of the disk (cf. Carollo et al. 1997; Devereux et al. 1997).

6. COMMENTS ON POSSIBLE FORMATION AND EVOLUTIONARY SCENARIOS FOR COMPACT STAR CLUSTER NUCLEI IN EXTREME LATE-TYPE SPIRALS

A possible clue to the origin of star cluster nuclei in extreme late-type spirals comes from the observation of van den Bergh (1995) that nuclei are *not* seen in irregular galaxies, even when these galaxies are of similar luminosities to the objects studied here. Artyukh & Ogannisyan (1991) also noted that compact nuclear radio sources (indicators of nuclear activity) are not generally found in irregular galaxies. This hints that somehow the presence of an organized

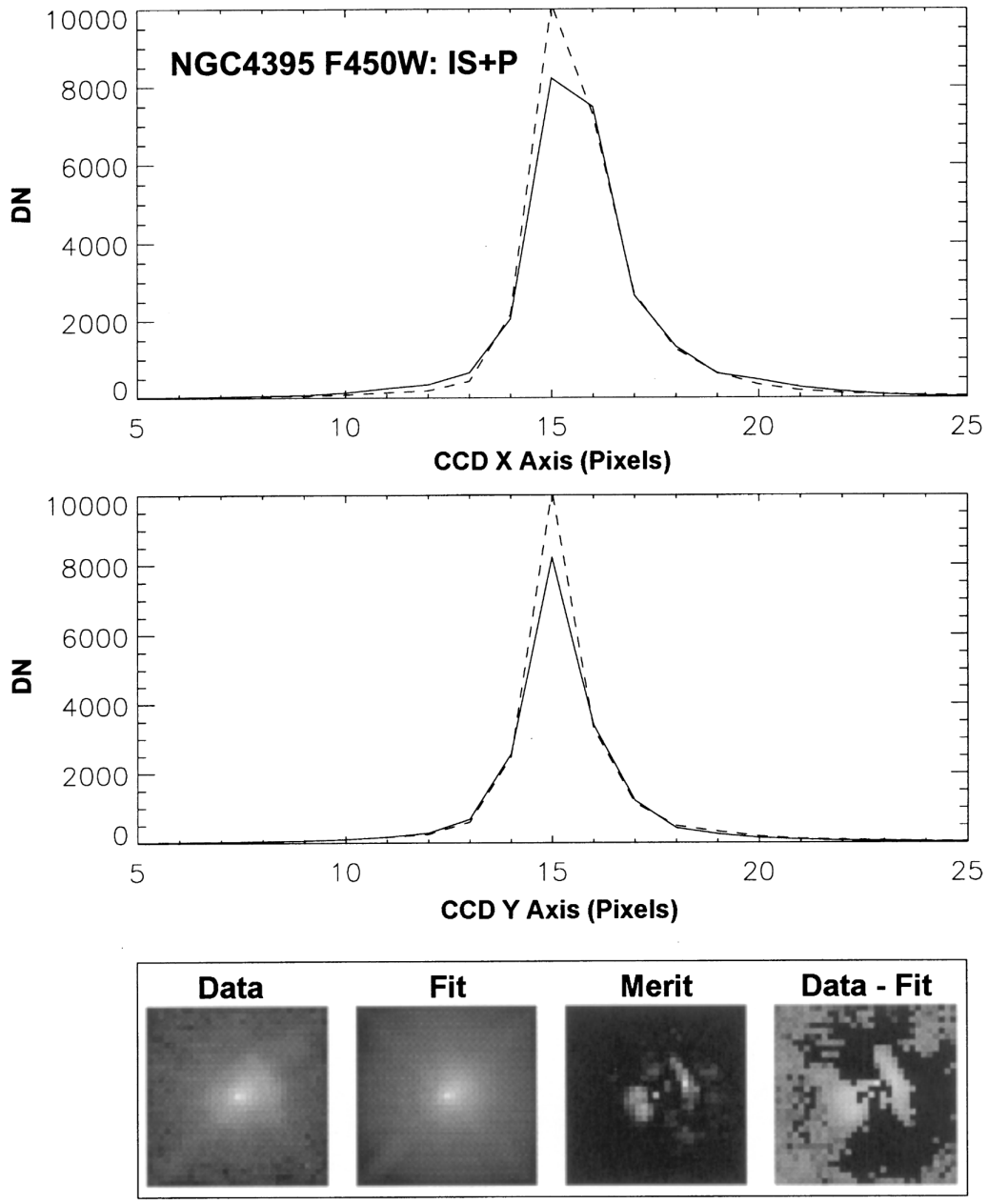

FIG. 17.—Same as Fig. 16, but only for the F450W image. Note the stronger intensity of the bipolar residual pattern compared with that seen in Fig. 16 for the F814W image.

disk is a requisite factor for the presence of a compact nucleus.

The rotation curves of extreme late-type spirals tend to be almost linear to the last measured point in the optical galaxy and to have very shallow velocity gradients (e.g., Goad & Roberts 1981; Wevers 1984; Matthews 1998). This indicates that the centers of these galaxies are not particularly "special" places and that they have relatively flat gravitational potential wells (see also Colin & Athanassoula 1981). This point was also emphasized by KM and Filippenko & Sargent (1989) for the cases of M33 and NGC 4395, respectively. By contrast, nucleated galaxies with luminous bulge components generally have steep density profiles with potentials pointing sharply toward their centers. There is some uncertainty whether the nuclei of our sample galaxies are even located precisely at the dynamical centers of these galaxies (see also Miller & Smith 1992). Minniti, Olszewski, & Rieke (1993) noted that the nucleus of M33 is displaced by $\sim 20''$ from its small "bulge" component, and it is also displaced from the center of true neighboring disk isophotes (de Vaucouleurs & Freeman 1972; Colin & Athanassoula 1981). In addition, the velocity centroid of the nucleus of ESO 359-029 appears to be displaced by ~ 7 km s^{-1} relative to the galaxy centroid (Matthews 1998). Taken together, the global and dynamical properties of nucleated extreme late-type spirals raise interesting new questions on the symbiosis between the nuclei and the parent galaxies and on the origin of these centralized mass concentrations in otherwise very diffuse disks.

Various models proposed for the formation of nuclei in early-type galaxies are problematic for the "naked" nuclei in extreme late-type spirals. Capuzzo-Dolcetta (1993) and Capuzzo-Dolcetta & Vignola (1997) have discussed the possibility that the nuclei of some early-type galaxies may

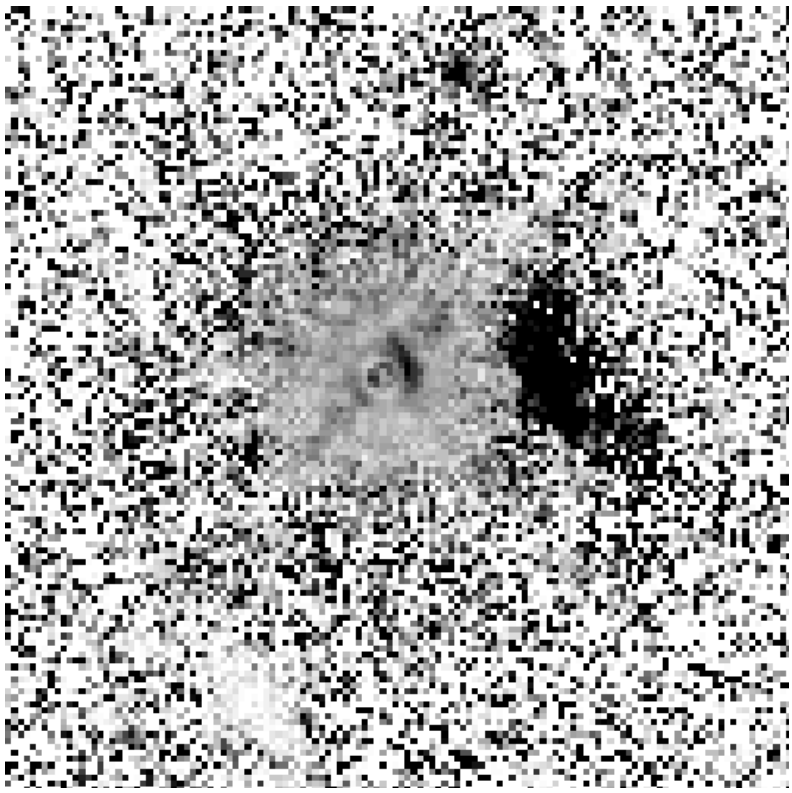

FIG. 18.—F450W − F814W color map of the NGC 4395 nucleus. The image size is roughly 6″.7 × 6″.7. Black areas are the bluest, and white areas are the reddest. The white elongated feature at the lower left-hand corner of the image is likely a background galaxy. Note the intense blue color of the plume on the left-hand side of the nucleus (seen more clearly in Fig. 20) and the small blue arc just to the right-hand side of the nucleus center.

form from globular clusters sinking to the center of the galaxies via dynamical friction. However, the efficiency of dynamical friction is greatly reduced in galaxies with low central densities (e.g., Lin & Tremaine 1983), making it doubtful that this scenario would be efficient in extreme late-type spirals. Finally, it appears that at least some extreme late-type spirals do not contain significant numbers of globular cluster systems (Matthews 1998).

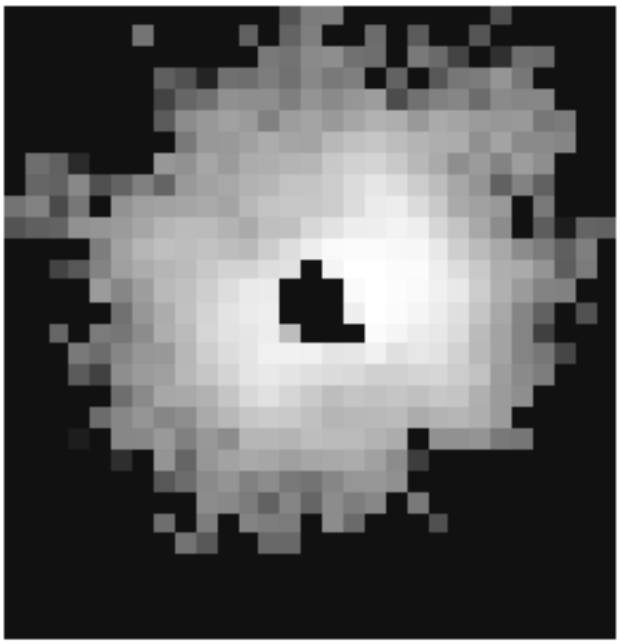

FIG. 19.—A 31 × 31 pixel image showing the residuals after subtraction of the best-fitting PSF from the NGC 4395 nucleus in the F450W image. Note the slight elongation of the residuals and the extra "bump" at roughly "2 o'clock" on the image.

Another possibility is that the nuclei formed in situ from gas infalling onto their centers because of either starbursts (e.g., Firmani & Tutukov 1994) or accretion of primordial gas clumps or small gas-rich galaxies (e.g., Loeb & Rasio 1994). While it seems plausible that infalling gas may have provoked episodic new star formation and altered the stellar populations of an *existing* nuclear star cluster in our galaxies (e.g., Firmani & Tutukov 1994; Tutukov & Krügel 1995), it is still difficult to explain how gas infalling into shallow potentials like those in extreme late-type spirals could have formed the compact star clusters at their centers. Less efficient angular momentum transport and weaker gravitational potentials in extreme late-type spirals provide a natural explanation for why they appear not to have formed supermassive black holes at their centers, but they cannot account for the extraordinary compactness of the nuclear star clusters. This conundrum was pointed out by KM with respect to M33. Our new data reveal that M33 is not an anomaly and that whatever the conditions necessary for the formation of a compact nucleus in extreme late-type spirals, these conditions commonly occur in these galaxies.

One possible means of delivering gas to galaxy centers to fuel activity or enhanced star formation is via a bar (e.g., Shlosman, Begelman, & Frenk 1990; Ho, Filippenko, & Sargent 1995b). Among our sample objects, NGC 4242 is generally classified as weakly barred, while none of the other galaxies, including M33, have obvious bars, and Ho (1996) also reported that bars do not appear to enhance the

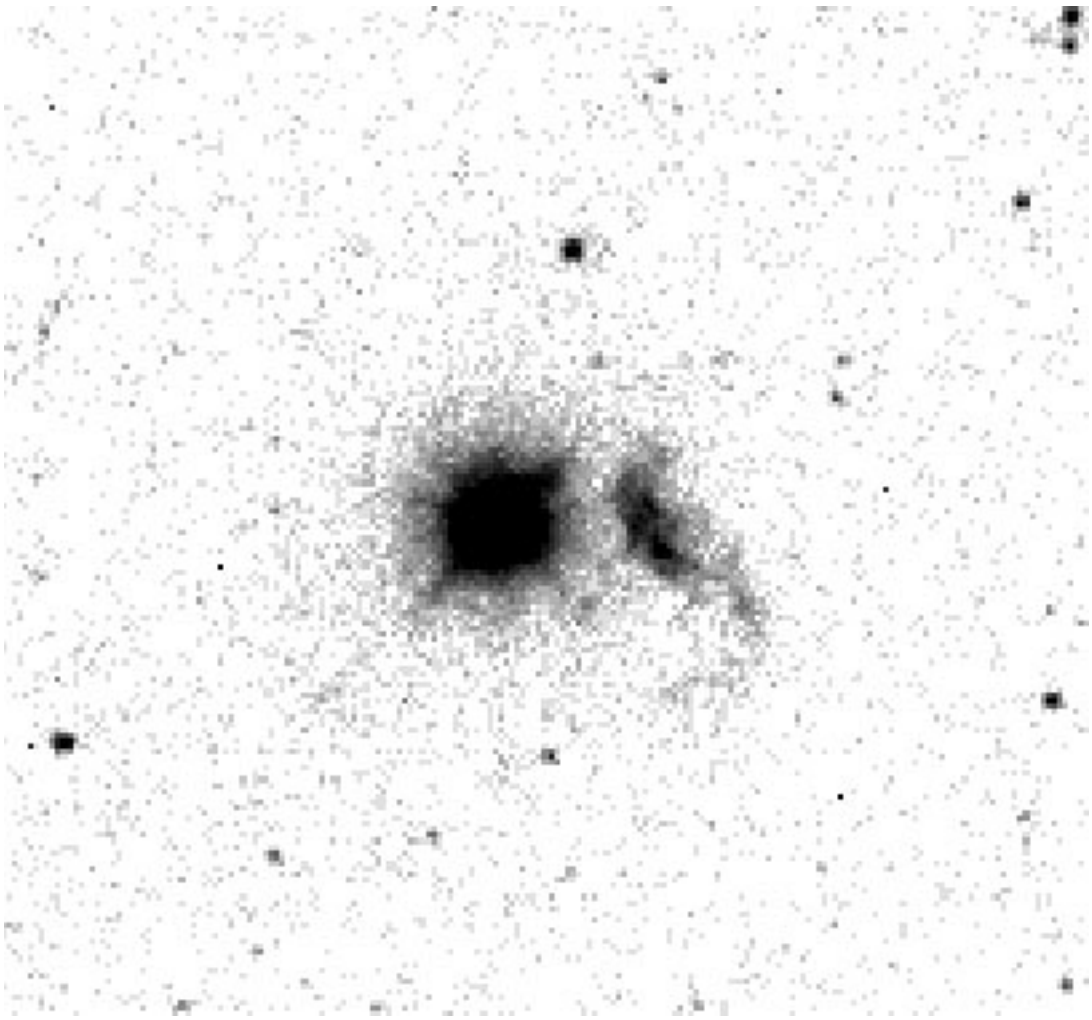

FIG. 20.—F450W image of the NGC 4395 nucleus. The image size is roughly 11.″6 × 11.″6. The gray scale is set to highlight the structure of the emission plume on the right-hand side of the nucleus. Two of the pixels near the center of the nucleus were saturated in this image and have been replaced by appropriately scaled values from our short exposure of this object (see § 2).

probability of finding a compact nucleus in galaxies later than Sbc (see also MacKenty 1990; Ho, Filippenko, & Sargent 1997c; Mulchaey & Regan 1997). However, it has been pointed out that secondary nuclear bars ~ 1 kpc in length may be needed to transport material effectively into the central parsec region of a galaxy (e.g., Shlosman, Frank, & Begelman 1989; Friedli & Martinet 1993). Such features have been detected in a few galaxies (Friedli et al. 1996), but we do not see any evidence of such bars in our program objects. We cannot, however, rule out that such structures may have existed in the past and aided the building of the observed nuclear star clusters.

Sofue & Habe (1992) suggested that late-type (Sc and Sd) galaxies may have been formed in low-density environments and suffered at most weak tidal interactions during their evolution. This explains the lower typical masses of these systems and their lack of large bulges. In this model, early-type galaxies formed in denser environments and developed bulges via tidally induced starburst events. If these interactions are also responsible for nucleus building and the fueling of AGNs (e.g., Loeb & Rasio 1994), this also could explain the lack of evidence for supermassive black holes in extreme late-type spirals. The low-level activity in NGC 4395 may have been caused by a very weak interaction or the accretion of a small, gas-rich satellite that was not enough to cause a significant alteration in the appearance of the galaxy. In the rare cases, such as the galaxy 0351+026, where an extreme late-type spiral is observed to harbor a more powerful active nucleus (see § 1.1), the tidal effects believed responsible for this activity (Bothun et al. 1982a, 1982b) may irrevocably change the appearance of the host galaxy, thus explaining the rarity of such objects in the present epoch. An alternative picture is that if primordial massive black holes are common in galaxies (e.g., Silk & Rees 1998), the presence of one in a galaxy may lead to "puffing" of the disk (e.g., Faber et al. 1997; Merritt 1998) and the formation of a bulge or spheroid; hence, by definition, none of these systems will be observed as extreme late-type spiral disks (cf. Matthews 1998).

M33 is the only case where our present data can help to constrain a more detailed model of the dynamical evolution of the nucleus. Because of its small velocity dispersion, the predicted relaxation time of the M33 nuclear star cluster is only $t_{\rm relax} \leq (2\text{–}3) \times 10^7$ yr (assuming $r_c = 0.1$ pc; Hernquist, Hut, & Kormendy 1991; KM). The colors of the M33 nucleus are also consistent with most of the stars being older than a relaxation time, so core collapse probably has occurred in M33. Our new upper bound to the radius of any

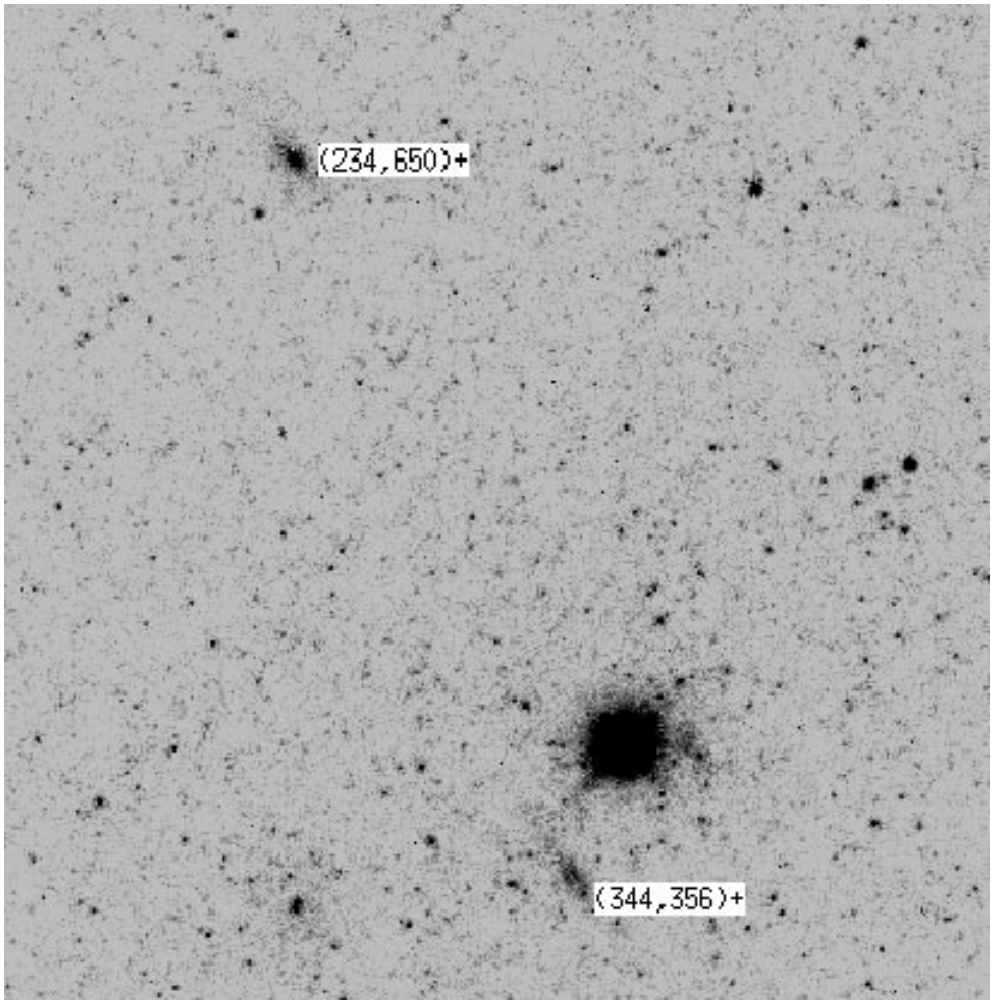

FIG. 21.—F814W image of the region around the NGC 4395 nucleus. The image is roughly 23″.2 × 23″.2. The coordinate boxes label what appear to be two background galaxies seen through the NGC 4395 disk. These features are not visible in the F450W image.

core in the nucleus of M33 strengthens this estimate of the relaxation time for simple models of core collapse (e.g., Spitzer & Hart 1971), although the effects of stellar encounters, stellar evolution, and a range of initial stellar masses may still create order-of-magnitude uncertainties in this value (KM; L98). Our measured value of the approximate core radius for our IS model component of the nucleus of M33 (0.11 pc) also agrees with theoretical predictions of the core-collapse scenario (Hernquist et al. 1991). L98 emphasize that stellar collisions may have particularly important consequences in the M33 nucleus, which lacks a supermassive black hole to stabilize its structure. However, it is likely that the structure of the M33 nucleus is more complex than that of an ordinary star cluster, and the detailed stellar mass density profile in the center of the nucleus is therefore still uncertain. These issues can be most directly resolved by spectroscopic observations designed to measure any radial trends in stellar content, possible signatures of a miniature AGN, and the nuclear kinematics.

7. DISCUSSION AND SUGGESTIONS FOR FUTURE WORK

We have shown that the nuclei of our program galaxies exist in similar, low-density galactic disk environments and have similar luminosities and spatial extents. All of these factors provide evidence (but not proof) that the four nuclei have shared common formation histories and are comprised of roughly similar underlying nuclear star clusters. We postulate that the color and morphological differences we observe among the various nuclei may be due to relatively short-lived evolutionary phases (e.g., episodes of enhanced star formation or nuclear activity) superposed on otherwise similar nuclear star clusters.

M33's nucleus is the only one of our program objects for which the dynamical information exists; hence, it is the only case for which a definite upper limit may be placed on the mass of a possible black hole at its center. We therefore know that any black hole in the nucleus of M33 must have a small mass ($M_{\rm BH} < 2 \times 10^4\ M_\odot$; KM; L98). Clearly, similar measures for the other program nuclei are needed to test further the hypothesis that the other nuclei in our sample resemble the nucleus of M33.

A velocity dispersion measure is of particular interest in the case of NGC 4395, since it can help to assess whether the activity in NGC 4395 is due to special properties or whether it represents a transient phase that M33 may have experienced in its past. Filippenko (1992) has estimated that if the nucleus of NGC 4395 contains a black hole accreting at roughly the Eddington limit, the black hole mass would only be $\sim 100\ M_\odot$. On the other hand, Filippenko points out that the formalism of Wandel & Yahil (1985) applied to

NGC 4395 yields an approximate black hole mass of $4 \times 10^4\ M_\odot$. This estimate assumes that the observed cloud speeds in the NGC 4395 nucleus are produced by gravity. This black hole mass estimate is nearly identical to the upper limit derived for M33 by KM and L98, so it is consistent with the nuclei of these two galaxies harboring similar central massive compact objects.

Further evidence for or against a "unified" picture for the nuclei of M33 and NGC 4395 could come from X-ray observations. Filippenko et al. (1993) quoted an unpublished X-ray luminosity of the NGC 4395 nucleus of 6.6×10^{37} ergs s^{-1}, which is consistent with the measurement obtained by Cui (1994). However, Lira & Lawrence (1998) report a mean $L_X \sim 9.7 \times 10^{37}$ ergs s^{-1} (for $D = 2.8$ Mpc) with a factor of 2 variability over a 15 day period. This is roughly a factor of 10 smaller than the X-ray luminosity of the M33 nucleus, but given the uncertainty in the distance to NGC 4395, and its slightly smaller total nuclear luminosity, it is conceivable that the X-ray luminosity of both M33 and NGC 4395 result from similar mechanisms. However, the reported X-ray variability occurs on timescales significantly shorter than the 106 day X-ray variability reported for the M33 nucleus by Dubus et al. (1997).

8. SUMMARY

We have analyzed WFPC2 broadband imaging observations of the compact star cluster nuclei of four extreme late-type spiral galaxies: M33, NGC 4395, NGC 4242, and ESO 359-029. All of these galaxies have diffuse, moderate-to-low surface brightness disks, low luminosities, little or no bulge component, and relatively weak central gravitational potentials. The nucleus of NGC 4395 is a previously known low-luminosity Seyfert 1 galaxy; M33 has some signs of possible weak activity, while the other two nuclei are not known to be active. However, we have confirmed that all four nuclei appear to be true compact star cluster nuclei rather than simply small nuclear H II regions.

All of the program nuclei are partially resolved with the Planetary Camera 2. The radial brightness profiles in all four nuclei cases are well fitted by a combination of an isothermal sphere (IS) and a central point-source (PSF) component, which we refer to as the "IS + P" model. Physically, this model implies that the structure of the nuclei may consist of an underlying star cluster with an abrupt change in luminosity density near the center. This gradient may be due to a power-law cusp in the stellar density profile, such as those associated with core collapse (e.g., L98), or could represent the presence of a pointlike source such as an AGN, a compact group of young stars, or a single supergiant star. The existence of an unresolved center in all of our program objects indicates that the luminosity densities in the centers of the nuclei are increasing to the resolution limit of our data.

In the case of M33, the IS + P model provides an equally good fit to the data as the continuous "nuker" power-law model of L98. Our choice of the simple IS + P model is physically motivated by the presence of a compact central light concentration in the Milky Way's nuclear cluster (seen superposed on a smoother nuclear star cluster background) and the inferred presence of AGNs *within* compact nuclear star clusters (e.g., Norman & Scoville 1988). A central subcluster of young stars like that in the Milky Way's nucleus would be at most marginally resolved by WFPC2 at the distance of M33, while an AGN would be unresolved (see Blandford 1990). The IS + P model therefore is on a firm physical basis for the NGC 4395 nucleus, where the point-source component represents an extremely compact AGN. More complex models can provide equally good or slightly better fits to the observed nuclear brightness maps, but these have more free parameters and provide at most small improvements in the fit accuracy. Furthermore, the more complex models could not be uniquely constrained and hence do not supply physically insightful information. While the IS + P model is simplistic, it is also well matched to the degree of resolution we can achieve for galaxy nuclei outside of the Local Group.

We show that because of the effects of increasing distance, the core radii we derive for the underlying nuclear star clusters of our program galaxies are only upper limits. We estimate the severity of the effects of distance on our measurements by producing an artificial "redshifted" version of the M33 nucleus. From that experiment, we conclude that the sizes of the compact star cluster components of all four of our program objects are similar to within a factor of 4, and all have core radii of less than 1.8 pc in the F814W band.

The luminosities of all four nuclei are similar ($M_I \sim -11 \pm 1$), indicating that nuclei with similar luminosities can be either active or nonactive. In spite of the modest range in optical luminosity, we see a spread of 1.81 mag in the $B-I$ colors of our program nuclei, with the active nucleus of NGC 4395 being by far the bluest. This spread in color may be indicative of different evolutionary phases (e.g., level of nuclear activity or recent star formation) in otherwise structurally similar underlying nuclei.

In spite of their compact sizes, the nuclei in our sample exhibit complex structure. M33 has slightly elliptical isophotes and shows the presence of a jetlike feature. This jetlike feature may be a signature of low-level activity in the M33 nucleus. NGC 4395 is even more structurally complex, especially in the F450W frame, where it appears as a point source superposed on elongated, somewhat irregularly shaped isophotes, possibly resulting from ionized gas emission. In addition, there is a bright arc very near the nucleus ($r \sim 3$ pc) that is likely due to [O III] emission, with $L(\mathrm{O\ III}) \approx 1 \times 10^4\ L_\odot$. A larger filamentary structure is found along the same line of sight at $r \sim 20$ pc and is also likely to be a highly ionized emission region. This pair of structures seems to be analogous to the "ionization cones" seen in more powerful AGNs. These features, in combination with the luminous blue point source that our model fits reveal, lend further support to a standard AGN model for the source of activity in the NGC 4395 nucleus (see also Filippenko et al. 1993). The similarity of the appearance of the NGC 4395 nucleus in the F814W filter to the other nuclei in our sample suggests that it is a fairly normal star cluster nucleus that happens to be presently hosting activity. Stellar velocity dispersion measurements will help to confirm or refute this picture.

NGC 4242 is the only one of the four program nuclei that appears more structurally complex in the F814W frame than in the blue image. Our IS + P model fits uncover an elongated bar-shaped residual structure at the center of this nucleus. ESO 359-029 appears relatively symmetric in our data, but this is the most poorly resolved of our program nuclei.

For the three nuclei for which we have F450W data, we measure IS model component core radii that are roughly

twice as large in the F814W band as in the F450W band. The blue luminosity therefore appears to be centrally concentrated, a symptom that could result from a variety of processes. As in the Milky Way's central star cluster, the star clusters in our program objects appear to have outlying populations of old or intermediate-age red stars and a larger mixture of stellar ages in their centers. The presence of miniature AGNs could also produce this trend, as would an excess population of "blue straggler" stars that could form via stellar mergers within dense nuclei (KM; L98).

Various factors make the origin of compact star cluster nuclei in small spiral galaxies enigmatic. Our new observations confirm that even when viewed at very high angular resolutions, all four of our program galaxies appear to be "naked"—that is, they exist in extremely diffuse circumnuclear environments with a low-density surrounding stellar disk, no spiral arms or significant bulge, few regions of enhanced star formation, and little indication of dust. These environments are in stark contrast to those typical of brighter compact nuclei and more powerful AGNs. In addition, the central gravitational potentials of the host galaxies of our program nuclei appear to be very shallow. Thus, it remains unclear how dense, compact collections of material formed at their centers. Furthermore, the morphologies of the host galaxies argue against their having been victims of major interactions (Matthews & Gallagher 1997), and their low central densities mitigate against dynamical friction being efficient enough for a star cluster formed elsewhere to migrate to the galaxy center.

L. D. M. has been funded by a graduate internship with the Wide Field Planetary Camera 2 Investigation Definition Team, which is supported at the Jet Propulsion Laboratory via the National Aeronautics and Space Administration under contract NAS 7-1260. This work has been carried out as part of the WFPC2 Investigation Definition Team science programs. We thank D. M. Peterson for comments on an earlier version of this manuscript.

REFERENCES

Artyukh, V. S., & Ogannisyan, M. A. 1991, Soviet Astron. Lett., 17, 377
Bevington, P. R. 1969, Data Reduction and Error Analysis for the Physical Sciences (New York: McGraw-Hill)
Binggeli, B. 1994, in Panchromatic View of Galaxies—Their Evolutionary Puzzle, ed. G. Hensler, Ch. Thies, & J. Gallagher (Gif-sur-Yvette: Editions Frontières), 173
Binggeli, B., & Cameron, L. M. 1991, A&A, 252, 27
Binggeli, B., Sandage, A., & Taraenghi, M. 1984, AJ, 89, 64
Binney, J., & Tremaine, S. 1987, Galactic Dynamics (Princeton: Princeton Univ. Press)
Biretta, J. A., et al. 1996, WFPC2 Instrument Handbook, Version 4.0 (Baltimore: STScI)
Blandford, R. D. 1990, in Active Galactic Nuclei, ed. T. J.-L. Courvoisier & M. Mayor (Berlin: Springer), 161
Boksenberg, A., et al. 1995, ApJ, 440, 151
Bothun, G. D., Mould, J., Heckman, T., Balick, B., Schommer, R. A., & Kristian, J. 1982a, AJ, 87, 1621
Bothun, G. D., Romanishin, W., Margon, B., Schommer, R. A., & Chanan, G. A. 1982b, ApJ, 257, 40
Bouyoucef, K., Fraix-Burnet, D., & Roques, S. 1997, A&AS, 121, 575
Capuzzo-Dolcetta, R. 1993, ApJ, 415, 616
Capuzzo-Dolcetta, R., & Vignola, L. 1997, A&A, 327, 130
Carollo, C. M., Stiavelli, M., de Zeeuw, P. T., & Mack, J. 1997, AJ, 114, 2366
Colin, J., & Athanassoula, E. 1981, A&A, 97, 63
Colina, L., Vargas, M. L. G., Mas-Hesse, J. M., Alberdi, A., & Krabbe, A. 1997, ApJ, 484, L41
Crane, P., et al. 1993, AJ, 106, 1371
Cui, W. 1994, Ph.D. thesis, Univ. Wisconsin, Madison
de Vaucouleurs, G. 1948, Ann. d'Astrophys., 11, 247
de Vaucouleurs, G., & Freeman, K. C. 1972, Vistas Astron., 14, 163
Devereux, N., Ford, H., & Jacoby, G. 1997, ApJ, 481, L71
Díaz, A. I., Pagel, B. E. J., Edmunds, M. G., & Phillips, M. M. 1982, MNRAS, 201, 49P
Dubus, G., Charles, P. A., Long, K. S., & Hakala, P. J. 1997, ApJ, 490, L47
Eckart, A., Genzel, R., Hofmann, R., Sams, B. J., & Tacconi-Garman, L. E. 1993, ApJ, 407, L77
Fabbiano, G., Fassnacht, C., & Trinchieri, G. 1994, ApJ, 434, 67
Faber, S. M., et al. 1997, AJ, 114, 1771
Filippenko, A. V. 1989, in IAU Symp. 134, Active Galactic Nuclei, ed. D. E. Osterbrock & J. S. Miller (Dordrecht: Kluwer), 495
———. 1992, in ASP Conf. Ser. 31, Relationships between Active Galactic Nuclei and Starburst Galaxies, ed. A. V. Filippenko (San Francisco: ASP), 253
Filippenko, A. V., Ho, L. C., & Sargent, W. L. W. 1993, ApJ, 410, L75
Filippenko, A. V., & Sargent, W. L. W. 1985, ApJS, 57, 503
———. 1989, ApJ, 342, L11
Firmani, C., & Tutukov, A. V. 1994, A&A, 288, 713
Ford, H. C., Caganoff, S., Kriss, G. S., Tvetanov, Z., & Evans, I. N. 1992, BAAS, 24, 818
Ford, H. C., Tsvetnanov, Z. I., Ferrarese, L., & Jaffe, W. 1998, in IAU Symp. 184, The Central Regions of the Galaxy and Galaxies, ed. Y. Sofue (Dordrecht: Kluwer), 377
Freedman, W. L., Wilson, C. D., & Madore, B. F. 1991, ApJ, 372, 455
Friedli, D., & Martinet, L. 1993, A&A, 277, 27
Friedli, D., Wozniak, H., Rieke, M., Martinet, L., & Bratschi, P. 1996, A&AS, 118, 461
Gallagher, J. S., Goad, J. W., & Mould, J. R. 1982, ApJ, 263, 101
Gioia, I. M., & Fabbiano, G. 1987, ApJS, 63, 771
Goad, J. W., & Roberts, M. S. 1981, ApJ, 250, 79
Hasan, H., & Burrows, C. J. 1995, PASP, 107, 289
Heckman, T. M. 1980, A&A, 87, 152
Hernquist, L., Hut, P., & Kormendy, J. 1991, Nature, 354, 376
Ho, L. C., Filippenko, A. V., & Sargent, W. L. W. 1995a, ApJS, 98, 477
———. 1995b, in IAU Colloq. 157, Barred Galaxies, ed. R. Buta, B. G. Elmegreen, & D. A. Crocker (San Francisco: ASP), 188
———. 1997a, ApJS, 112, 315
———. 1997b, ApJ, 487, 568
———. 1997c, ApJ, 487, 579
Holtzman, J. A., et al. 1995a, PASP, 107, 156
Holtzman, J. A., Burrows, C. J., Casertano, S., Hester, J. J., Trauger, J. T., Watson, A. M., & Worthy, G. 1995b, PASP, 107, 1065
Hubble, E. P. 1930, ApJ, 71, 231
Jones, D. H., et al. 1996, ApJ, 466, 742
King, I. 1962, AJ, 67, 471
———. 1966, AJ, 71, 64
King, I. R., Stanford, S. A., & Crane, P. 1995, AJ, 109, 164
Koratkar, A., Deustua, S. E., Heckman, T., Filippenko, A. V., Ho, L. C., & Rao, M. 1995, ApJ, 440, 132
Kormendy, J., & McClure, R. D. 1993, AJ, 105, 1793 (KM)
Krabbe, A., et al. 1995, ApJ, 447, L95
Krist, J. 1996, Tiny Tim Users Manual, Version 4.1 (Baltimore: STScI)
Kunth, D., Sargent, W. L. W., & Bothun, G. D. 1987, AJ, 93, 29
Lauberts, A., & Valentijn, E. A. 1989, The Surface Photometry Catalogue of the ESO-Uppsala Galaxies (Garching: ESO)
Lauer, T. R., et al. 1993, AJ, 106, 1436
———. 1995, AJ, 110, 2622
Lauer, T. R., Faber, S. M., Ajhar, E. A., Grillmair, C. J., & Scowen, P. A. 1998, AJ, 116, 2263 (L98)
Light, E. S., Danielson, R. E., & Schwarzschild, M. 1974, ApJ, 194, 257
Lin, D. N. C., & Tremaine, S. 1983, ApJ, 264, 364
Lira, P., & Lawrence, A. 1998, in IAU Symp. 184, The Central Regions of the Galaxy and Galaxies, ed. Y. Sofue (Dordrecht: Kluwer), 83
Loeb, A., & Rasio, F. A. 1994, ApJ, 432, 52
Lyutyi, V. M., & Sharov, A. S. 1990, Soviet Astron. Lett., 16, 376
MacKenty, J. W. 1990, ApJS, 72, 231
Maiolino, R., & Rieke, G. H. 1995, ApJ, 454, 95
Maoz, D., Filippenko, A. V., Ho, L. C., Rix, H.-W., Bahcall, J. N., Schneider, D. P., & Macchetto, F. D. 1995, ApJ, 440, 91
Marquardt, J. 1963, J. SIAM, 11, 431
Massey, P., Bianchi, L., Hutchings, J. B., & Stecher, T. P. 1996, ApJ, 469, 629
Matthews, L. D. 1998, Ph.D. thesis, State Univ. New York, Stony Brook
Matthews, L. D., & Gallagher, J. S. 1997, AJ, 114, 1899
Matthews, L. D., Gallagher, J. S., Krist, J., Burrows, C., and WFPC2 Investigation Definition Team. 1996, BAAS, 28, 824
Matthews, L. D., van Driel, W., & Gallagher, J. S. 1998, AJ, 116, 1169
Merritt, D. 1998, Comments Astrophys., 19, 1
Mezger, P. G., Duschl, W. J., & Zylka, R. 1996, A&A Rev., 7, 289
Michard, R. 1996, A&AS, 117, 583
Mighell, K. J., & Rich, R. M. 1995, AJ, 110, 1649
Miller, R. H., & Smith, B. F. 1992, ApJ, 393, 508
Minniti, D., Olszewski, E. W., & Rieke, M. 1993, ApJ, 410, L79
Mould, J. R., Graham, J., Matthews, K., Soifer, B. T., & Phinney, E. S. 1989, ApJ, 339, L21
Mulchaey, J. S., & Regan, M. W. 1997, ApJ, 482, L135
Mulchaey, J. S., Wilson, A. S., & Tsvetanov, Z. 1996, ApJ, 467, 197
Nieto, J.-L., & Aurière, M. 1982, A&A, 108, 334

Nieto, J.-L., Macchetto, F. D., Perryman, M., Di Serego Aliighieri, & Lelièvre, G. 1986, A&A, 165, 189
Norman, C., & Scoville, N. 1988, ApJ, 332, 124
O'Connell, R. W. 1983, ApJ, 267, 80
Oosterloo, T., Da Costa, G. S., & Staveley-Smith, L. 1996, AJ, 112, 1969
Perry, J. J., & Williams, R. 1993, MNRAS, 260, 437
Phillips, A. C., Illingworth, G. D., MacKenty, J. W., & Franx, M. 1996, AJ, 111, 1566
Pişmiş, P. 1987, Rev. Mexicana Astron. Astrofis., 14, 108
Pogge, R. W. 1989a, AJ, 98, 124
———. 1989b, ApJ, 345, 730
Regan, M. W., & Mulchaey, J. S. 1998, BAAS, 29, 1333
Reynolds, J. H. 1913, MNRAS, 74, 132
Rieke, G. H., & Rieke, M. J. 1994, in The Nuclei of Normal Galaxies, ed. R. Genzel & A. I. Harris (Dordrecht: Kluwer), 283
Rowan-Robinson, M. 1985, The Cosmological Distance Ladder (New York: Freeman)
Rubin, V. C., & Ford, W. K., Jr. 1986, ApJ, 305, L35
Sams, B. J., III. 1995, ApJ, 445, 221
Sandage, A., & Bedke, J. 1994, The Carnegie Atlas of Galaxies (Washington: Carnegie Inst. Washington)
Sandage, A., & Fomalont, E. 1993, ApJ, 407, 14
Sarajedini, V. L. 1996, BAAS, 189, No. 109.02
Sarajedini, V. L., Green, R. F., Griffiths, R. E., & Ratnatunga, K. 1996, ApJ, 471, L15
Schmidt, A. A., Bica, E., & Alloin, D. 1990, MNRAS, 243, 620
Schmitt, H. R., & Kinney, A. L. 1996, ApJ, 463, 498
Schulman, E., & Bregman, J. N. 1995, ApJ, 441, 568
Sharov, A. S., & Lyutyi, V. M. 1988, Soviet Astron., 32, 469
Shields, J. C., & Filippenko, A. V. 1992, in ASP Conf. Ser. 31, Relationships between Active Galactic Nuclei and Starburst Galaxies, ed. A. V. Filippenko (San Francisco: ASP), 267
Shlosman, I., Begelman, M. C., & Frenk, J. 1990, Nature, 345, 679
Shlosman, I., Frank, J., & Begelman, M. S. 1989, Nature, 338, 45
Silk, J., & Rees, M. J. 1998, A&A, 331, L1
Sofue, Y., & Habe, A. 1992, PASJ, 44, 325
Spitzer, L., & Hart, M. H. 1971, ApJ, 164, 399
Sramek, R. 1992, in ASP Conf. Ser. 31, Relationships between Active Galactic Nuclei and Starburst Galaxies, ed. A. V. Filippenko (San Francisco: ASP), 273
Terlevich, R., & Melnick, J. 1985, MNRAS, 213, 841
Tutukov, A. V., & Krügel, E. 1995, A&A, 299, 25
Trauger, J., et al. 1994, ApJ, 435, L3
Tully, R. B. 1988, Nearby Galaxies Catalog (Cambridge: Cambridge Univ. Press)
van den Bergh, S. 1976, ApJ, 203, 764
———. 1991, PASP, 103, 609
———. 1995, AJ, 110, 613
van der Kruit, P. C. 1987, A&A, 173, 59
van der Marel, R. P. 1998, in IAU Symp. 186, Galaxy Interactions at Low and High Redshift, ed. D. B. Sanders & J. Barnews (Dordrecht: Kluwer)
Walker, M. 1964, AJ, 69, 744
Wandel, A., & Yahil, A. 1985, ApJ, 295, L1
Wang, J., Heckman, T. M., & Lehnert, M. D. 1997, ApJ, 491, 114
Watson, A. M., et al. 1996, AJ, 112, 534
Wevers, M. H. R. 1984, Ph.D. thesis, Univ. Groningen
Wildey, R. L. 1992, PASP, 104, 285
Williams, R. J. R., & Perry, J. J. 1994, MNRAS, 269, 538
Wilson, A. S., Braatz, J. A., Heckman, T. M., Krolik, J. H., & Miley, G. K. 1993, ApJ, 419, L61